

Intraspecific Variation of Endocranial Structures in Extant *Equus*: A Prelude to Endocranial Studies in Fossil Equoids

Endocranial Intraspecific Variation in *Equus*

Laure Danilo¹ · Jean Remy² · Monique Vianey-Liaud¹ · Samuel Mérigeaud³ · Fabrice Lihoreau¹

Published online: 8 April 2015
© Springer Science+Business Media New York 2015

Abstract Intraspecific variation of endocranial structures is not widely studied in most mammals, particularly fossil mammals, which are mainly represented by a few preserved crania. However, a description of this variation is necessary to be able to study fossil mammals from an ecological and phylogenetic perspective. To facilitate further analyses on fossil equoids, digital reconstructions of the cranial endocast, petrosal bone, and bony labyrinth were created based on CT scans, taken from a wild population of 12 *Equus caballus przewalskii* currently being monitored. Using descriptive, biometric, and morphometric analyses, an unsuspected range of intraspecific variation for 40 endocranial characters is revealed. Intraindividual variation can be further understood through the comparison of paired organs from a single individual. These results prompt cautious consideration of these characters, as well as an index for the determination of hearing abilities or encephalization quotients.

Thanks to this work, more is now known about the intraspecific variation of the external morphology of the most frequently studied structures in the endocranium of mammals and more specifically in equoids, where no such study had

been undertaken until now. This will help to improve the resolution of fossil endocranial studies.

Keywords Intraspecific variation · Digital cranial endocast · Petrosal · Bony labyrinth · Przewalski horse · Equoids

Introduction

Studies of fossil endocranial structures require well-preserved crania but such fossil materials are scarce. These structures have long been studied from anecdotal records of natural endocasts (e.g., Cuvier 1836; Weinberg 1903; Dietrich 1936; Edinger 1948; Dechaseaux 1962; Radinsky 1967; Jerison 1973; Novacek 1982). With the advent of computed tomography, endocranial structures now represent a renewed source for fossil description (e.g., Rowe et al. 1999, 2011; Brochu 2000; Witmer et al. 2003; Macrini et al. 2007a; Dong 2008; Silcox et al. 2009; David et al. 2010; Orliac et al. 2012; Benoit et al. 2013b; Ekdale 2013). Underestimating variation often leads to a poor and likely biased definition of fossil taxa (e.g., Horner and Goodwin 2009; Scannella and Horner 2010). This statement is particularly true for the bony labyrinth, which is almost unreachable without a CT scan. However, the intraspecific variation of these structures is still not well known; only a few papers have begun to explore the issue (e.g., on metatherians, Macrini et al. 2007b; on a large sample of mixed fossil species of oreodonts, Macrini 2009; on the ontogeny of a metatherian, Ekdale 2010; on a petrosal sample of elephant relatives, Ekdale 2011; on six porpoises, Racicot and Colbert 2013). The variation cannot be generalized to all mammals based on such a limited number of studies. In order to identify the intraspecific variation of the external morphology of endocranial structures in eutherian mammals, it is first necessary to track said variation within extant populations by

Electronic supplementary material The online version of this article (doi:10.1007/s10914-015-9293-x) contains supplementary material, which is available to authorized users.

✉ Laure Danilo
laure.danilo@univ-montp2.fr

¹ Institut des Sciences de l'Évolution de Montpellier (ISEM) – UMR CNRS 5554, Université de Montpellier, CNRS, IRD, EPHE, Place Eugène Bataillon, FR–34095 Montpellier cedex 05, France

² 46 rue Rouget de Lisle, 30000 Nîmes, France

³ Centre de Radiologie, Clinique du Parc, Castelnau Le Lez, France

clearly pointing out which structures vary and in what proportions. Such groundwork was undertaken for this paper, defining the morphological space of endocranial structures in an extant perissodactyl, the Przewalski's horse, *Equus caballus przewalskii* Poliakov, 1881. The internal structures of the cranium were studied non-invasively (cranial endocast, petrosal bone, bony labyrinth, and sinuses) through X-ray computed tomography (CT), relying on comparative anatomy and three-dimensional morphometric geometry. The sample helped to call into question the use of the encephalization quotient and the validity of current comparisons between different quotients. The variability between both sides of a paired organ from a single individual was also tested. By cautiously discriminating between endocranial characters, this analysis will help to describe and compare endocranial fossils of Equoidea for phylogenetic and paleobiological purposes in future studies. Such knowledge paves the way to suggesting new, robust characters that could allow the diagnosis of fossil specimens lacking teeth. Above all it could bring more phylogenetic resolution to controversial groups such as fossil equoids (Savage et al. 1965; Remy 1967; Franzen 1968; Hooker 1989, 1994; Froehlich 1999; Danilo et al. 2013).

Material and Methods

Material

In order to investigate intraspecific variation, it is essential to sample a single, homogenous population. Without this precaution, there is a possibility of bias variation due to geographic dispersal or to artificial selection, as found between breeds of domestic horses. Among extant equids this is a real challenge because of the great impact of artificial selection on various populations of horses and donkeys. Moreover, species of zebras are not well defined (Oakenfull et al. 2001; Oakenfull and Ryder 2002) and hardly available. Therefore, a population of another extant equid, the Przewalski's horse, was chosen.

Although extant populations of *Equus caballus przewalskii* live in the wild and exhibit natural behavior, it seems that a century spent in captivity has led to morphological modifications. The last truly wild individual lived somewhere around the 1960s. Today, all individuals of this sub-species are born of captive horses. Several authors have shown that domestication generally leads to a decrease in the size of the braincase and the brain in different species, without a return to feralization (Gorgas 1966; Kruska 1973, 1982, 1987, 1988, 2005, 2007; Röhrs and Ebinger 1993, 1998). Even though Przewalski's horse was never domesticated in a similar way to the common domestic horse, its captivity did last for a century. Moreover, hybridization between *E. c. przewalskii* and *E. c. caballus* Linnaeus, 1758, certainly occurred during the century when the former was only living in captivity, as

well as in the wild (Mohr 1959; Röhrs and Ebinger 1993; Volf 2003); though in a recent analysis, Orlando et al. (2013) found no genetic evidence of recent admixture. According to Gorgas (1966), Kruska (1973), or Röhrs and Ebinger (1993, 1998) and their measurements of endocranial cavity size, this is sufficient to lead to changes in brain size.

In spite of life in the wild and their natural behaviors, *E. c. przewalskii* can no longer be considered a pure blood wild equid. All of the studies on the consequences of domestication on the brain indicate only changes in brain volume. This is not the main focus here. In spite of evidence of domestication, the Przewalski's horse is still the best available model for such a study because no large collection of skulls from a single and homogenous population of real wild equids, like zebras, was available. Furthermore, *E. c. przewalskii* displays a limited range of body sizes and therefore of braincase and brain sizes, compared to *E. c. caballus* (body sizes ranging from 0.35 to 2 m high). Finally, populations of *E. c. przewalskii* have morphological and molecular homogeneity (Achilli et al. 2012).

With *E. c. przewalskii*, it became possible to choose material from a population under close scrutiny and yet deprived of human interaction. This provided a large amount of information on topics such as sex, age, and behavior. These data could then be used to investigate the origin of the variation as observed. The material comes from the TAKH association, "takh" being the Mongolian name of *E. c. przewalskii*, which deals with reintroduction of Przewalski's horses in Mongolia. Since 1990, they have bred about 30 horses in relative freedom on 400 ha of land, without contact with humans, in the "Causse Méjean" (southern France, 130 km northwest of Montpellier). The TAKH association provided 12 well-preserved crania of their dead Przewalski's horses, one of which lacks its petrosal bones. All of these have been scanned (Table 1). Each specimen is sexed and aged and their ethological data and genealogical relationships within the population are known (see Online Resource 1 for genealogy relationships).

As a result, these horses seem to be the best model to explore intraspecific variation in equoids.

In the reconstructions of *E. c. przewalskii*, endocranial structures of interest are the digital cranial endocast, bony labyrinth, and temporal sinus because of their implications for neurocranial soft tissues such as the brain, inner ear, and venous sinuses. As part of the neurocranium, the petrosal bone was also studied because of its close relation with the inner ear and the brain against which it is closely placed. Jerison (2007) noted that the endocranial cavity generally reproduces many details of the convolutions of the brain. However, previous papers have shown significant differences between a brain and its endocranial cavity in certain mammals (e.g., in the elephant: Shoshani et al. 2006; Manger et al. 2009). These differences concern imprints left by the encephalic convolutions on the skull roof, especially in the case of very thick meninges.

Table 1 Material studied. All specimens are *Equus caballus przewalski* except UM N669 and UM N675 which are *Equus caballus caballus*, providing the two freshly cut heads

Specimen	Sex	Age (years)	Ethological data	Group	R. brain (mm)	R. petrosal (mm)	R. inner ear (mm)	R. sinus (mm)	S. brain	S. inner ear
AR	M	1.2	Non established (young)	1	0.488	/	/	/	433	/
BB	M	3.5	Non established (young)	1	0.488	0.488	0.488	0.488	514	105
BE	F	10.3	Dominant mare	1	0.488	0.234	0.234	0.488	792	185
CE	F	5.8	Subordinate to three mares	2	0.498	0.498	0.498	0.498	540	/
EH	F	2.2	Non established (young)	2	0.488	0.234	0.234	0.488	756	157
EL	F	14	Second dominant mare (after BE)	2	0.523	0.293	0.293	0.523	646	144
EM	F	3.9	Non established (young)	2	0.488	0.215	0.215	0.488	727	155
MA	M	10.8	Dominant stallion	2	0.523	0.383	0.383	0.523	667	131
PN	M	3.2	Non established (young)	1	0.523	0.303	0.303	0.523	628	159
SC	F	3.4	Non established (young)	2	0.488	0.488	0.488	0.488	519	89
SI	F	2	Non established (young)	2	0.410	0.230	0.230	0.410	598	123
SN	M	3.8	Non established (young)	2	0.488	0.488	0.488	0.488	628	127
UM N669	?	?	/	/	0.848	0.848	0.848	0.848	70	/
UM N675	?	?	/	/	0.848	0.848	0.848	0.848	69	/

Group column represents synthetic genealogical relationships, with two distinct group of individuals, R, CT scan resolution; S, number of slices; ?, unavailable data; /, inapplicable data

In order to compare soft tissue morphology and more specifically real brains and sinuses to digital reconstructions based upon the endocranial cavity in a given individual, two freshly cut heads of *E. c. caballus* were also studied.

X-Ray Tomography

When dealing with fossils, it is necessary to reconstruct the cranial cavity to estimate the morphology and measurements of the brain from the internal surface of the bones of the skull. These are available using X-ray computed tomography (CT) technology, providing the virtual cross-sections. The same analysis was also performed on the extant Przewalski crania. They were scanned at the University Hospital Center Lapeyronie (CHU-Lap) of Montpellier (France) using a MultiDetector CT scanner General Electric Lightspeed VCT (Table 1). The two freshly cut heads were scanned in the veterinary clinic of Celleneuve (Montpellier, France). All of these structures were then reconstructed with the Avizo software (version 7, 2010), using both manual and semi-automatic segmentation.

Biometry

For digital cranial endocasts, the nomenclature was described in Fig. 1 and for digital petrosals and bony labyrinths in Fig. 4.

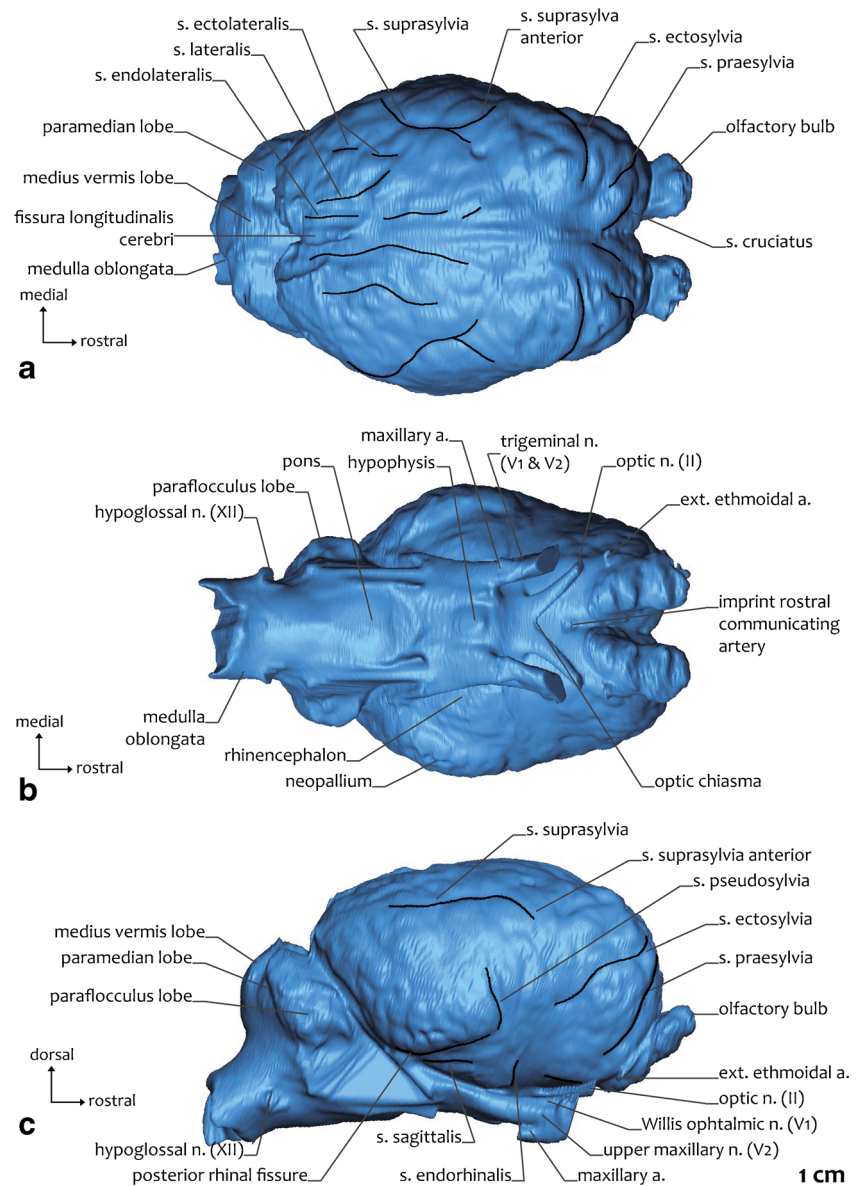
Several volumes were defined using the Avizo software to estimate proportions between the cerebrum, cerebellum, and olfactory bulbs. The cerebellum outlines are barely identifiable on the scans; therefore the measured volume is defined

taking into account the anatomy of an actual brain (Fig. 1). To calculate the volume of the whole endocast, the virtual endocast was conventionally delimited at the back by the emergence of the hypoglossal nerve (Fig. 1), excluding the rest of the medulla oblongata.

Using an arbitrarily determined line as a reference, several distances were measured to describe the arrangement of nerves of the orbit. This line, called “trigeminal emergence,” joins the two points where, from a ventral view, both trigeminal nerves emerge from the digital endocast (Online Resource 2). The proportions between the neopallium and the rhinencephalon were also estimated using the N/C index, the ratio between neopallium height and cerebrum height (Online Resource 2). Other measurements taken are explained in Online Resource 2 (A-E), as are those of the petrosal bone (G) and bony labyrinth (H, I). To supplement the sample, both left and right petrosals and bony labyrinths in 11 out of 12 specimens of *E. c. przewalskii* were reconstructed. One (AR) was damaged and did not retain these structures. As the skulls were scanned at a low resolution (hospital CT scan), the definition of these tiny structures was poor. Angles between semicircular canals were measured when they both were visible from the top, which is when their planes are orthogonal to the plane of the screen capture. As currently practiced (e.g., Geisler and Luo 1996; Orliac et al. 2012; Ekdale 2013; Benoit et al. 2013a), the number of turns of the cochlear canal can be determined when the field of view shows the bottom of the axis of rotation.

Lastly came the correlation by Manoussaki et al. (2008) linking the cochlear shape to limits in low-frequency hearing. They showed that the radii ratio of the cochlea (ratio between

Fig. 1 Digital reconstructions of *Equus caballus przewalskii* brain (specimen SN). **a** Dorsal view. **b** Ventral view. **c** Left lateral view. *a*, artery; *ext*, external; *n*, nerve; *s*, sulcus



radius of the basal turn and apical turn) could describe part of the shape of the cochlea involved in low-frequency hearing.

Encephalization Quotients

Two encephalization quotients were calculated so as to estimate the relative brain size of *E. c. przewalskii*. Both methods are based on an estimation of the brain weight (E_c), which can be derived from the body weight (EQ, Jerison 1973) or from the foramen magnum surface (EQA, Radinsky 1967, 1976) (Online Resource 2C).

Again, in order to standardize this approach, the same body weight estimations were made as would be made on fossil material. For extinct species, body weight can be estimated from teeth measurements or animal body length (approximated by the skull length). Both methods are used and compared

in this work. Janis (1990) defined equations on perissodactyls and hyracoids to link teeth measurements and body weight. Given that the whole sample used in this work comprises eight young horses without M3/m3 teeth, six of these variables from the lower and the upper teeth were used to calculate an average body weight. In order to compare these values to fossil material in future studies where the lower teeth are rarely associated to the cranium, the body weight was also calculated using only the two upper teeth measurements. Conversely, the assessment of body length based on skull length was done by comparison of this ratio in extant Equoidea as provided by several authors (Simpson 1951; Bourdelle in Viret 1958; Barone 2004; Franzen 2010). The total body length is considered equal to the skull length plus the neck length and the main body length. The average ratio obtained was 4.54 for skull length/body length for Przewalski's horses. Remy (1978,

2004) defined equations from Walker's data (1968) that link body length and body weight. These data comprised 75 ungulate species and included numerous light and slender species such as some antelopes whose morphology is far removed from that of Equoidea. That is the reason Remy (1998, 2004) used a part of these data to define his equations. First, he considered the three quarters and a half of these species and obtained two formulae, $P_1 = 0.0084 * L^{3.27}$ and $P_2 = 0.019 * L^{3.15}$, where P and L represented respectively weight and length of the body. From these body weights, Jerison (1973) defined the equation $E = 0.12 P^{2/3}$ where P is still the body weight and E the estimated brain weight (E_c).

Radinsky (1976) showed that the surface of the foramen magnum is highly correlated to the body weight in five orders of mammals (excluding the Perissodactyla). From this correlation he defined the formula: $E = 22.4 A^{1.48}$ where E is the estimated brain weight (E_c) and A is the surface of the foramen magnum (Radinsky 1976).

The encephalization quotient was obtained by dividing the measured brain weight E_i (correctly approximated by the volume of its cavity (Remy 1972; Radinsky 1976)) by the expected brain weight E_c in an extant mammal of similar size, according to Jerison (1973) (EQ) or Radinsky (1967) (EQA). In all these calculations, like Radinsky (1967) and Jerison (1973), the volume of the cerebrum and the cerebellum plus the olfactory bulbs were considered, excluding the medulla oblongata which is caudal to the hypoglossal nerves.

Three-Dimensional Geometric Morphometry

In the case of complex morphologies, three dimensional, geometric, morphometric methods complement the more classical descriptive methods. It allows the quantitative description of the form and the observation of changes to the form, regardless of size. A landmarks protocol was defined for each studied structure and they were positioned with the Meshtools software (Lebrun et al. 2010), except the temporal sinus due to the few definable homologous points available. Semi-

landmarks were used to describe the curve of the cochlea. They consist of a succession of equidistant points, joined virtually by a line along the curve. According to Bookstein (1997) or Gunz et al. (2005), these points could require a transformation in order to maximize their homology. This sliding was performed with Morphotools software (Specht 2007; Specht et al. 2007; Lebrun et al. 2010). Then, a procrustes superimposition helped to overcome the differences of size, orientation, or position between all the specimens of the sample. Results of the procrustes superimposition were then used as variables in statistical multivariate analyses such as Principal Component Analysis. These superimposition and statistical analyses were performed with the Morphotools software. It allowed the visualization of the needed deformation to switch from one specimen to another and to define a virtual tri-dimensional morphological space from which all conceivable morphologies extended.

Results

Digital Reconstruction of the Cranial Endocast and Brain Morphology

The temporal sinus, the transverse sinus, and the communicating sinus crossing the temporal sinus all adhere closely to the brain. On CT scans of skulls, a single cavity encompassed all of these structures. They must therefore be delimited. Scans of the freshly cut heads allowed observation of the boundary between brain and sinuses, in those places where no bony wall exists. This information is essential for a good brain reconstruction, especially the occipital region and lateral sides of the brain (Fig. 2). Without such delimitation, an endocast reconstruction could easily include some parts of the large sinuses closely placed against the brain without the user noticing. Therefore, all endocasts were reconstructed using these new data and this will be extended to fossil equoids in further studies.

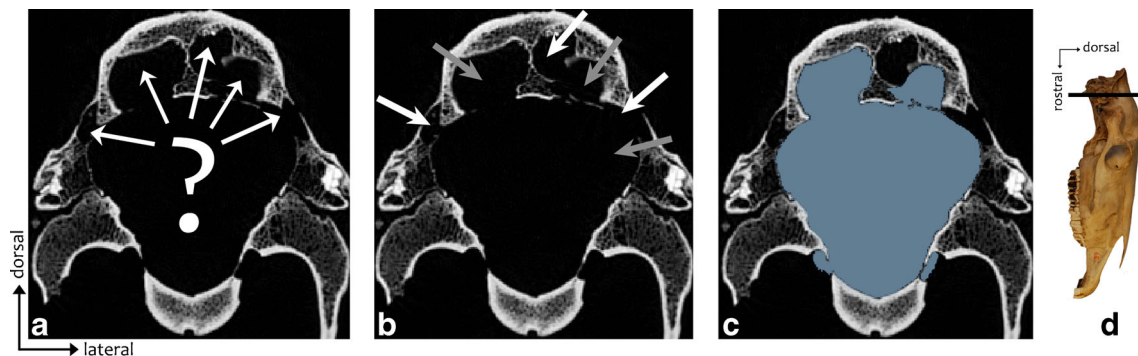


Fig. 2 Digital reconstruction versus real brain: what differences? CT scan virtual slides of *Equus caballus caballus* in coronal sections. **a** Neurocranial cavity is complex and made of numerous communicant cavities. **b, c** Segmentation of the brain from new delimitation data

allowed by study of the freshly cut heads. In **b**, white arrows show sinus whereas grey arrows point brain. **d** Lateral view of the cranium showing (black line) the location of the virtual slides

On these CT scans of freshly cut heads, the soft tissues (brain and meninges) displayed very similar density to X-rays. Therefore, these tissues were merged on the virtual slides and so it was impossible to examine the real morphology of the brain. As a consequence, the evaluation of the thickness of the meninges was not possible from these virtual slides. However, the observation of the morphology of cranial endocasts in both extant and extinct Equoidea led to the hypothesis of the similarity of the thickness of their meninges. In fact, on reconstructed endocasts of extant Equoidea, sulci and gyri are less distinct than on the fossil Equoidea for the posterior part of the neopallium but not, however, in the frontal lobes. Therefore this difference should not be due to the thickness of the meninges. In spite of its blurred appearance, it is possible to distinguish all the sulci on the posterior part of the neopallium of an extinct equoid, *Plagiolophus minor* (Cuvier, 1804) (Remy 1978, 2004, Online Resource 3) whereas only few are identifiable in Przewalski's horses (Fig. 1, Online Resource 3). However, the sharpness of the frontal lobes of the natural cranial endocast of *P. minor* resembles that in Przewalski's horses. The whole neopallium of *P. minor* is as blurred as the one from Przewalski's horses but the posterior part in *P. minor* seems more obvious because of the greater simplicity of the sulci (Online Resource 3). Indeed, these are straight in *P. minor*, whereas in Przewalski's horses their lines are very sinuous and this could explain the apparent difference between these endocasts. Located between the brain and the cranial bones, the meninges are the main cause of the blurred appearance in both. One of them, the dura mater, is very fibrous and rigid and conceals the brain's imprint on the cranial bones. It therefore prevents the reconstruction of the exact morphology of the brain, which explains the blurred appearance of the neopallium. Since the frontal lobes look similar, the thickness of the meninges is supposedly the same. The difference in the recognition of the sulci probably results from a difference in complexity. Indeed, it is easier to follow blurred straight lines than blurred, highly sinuous ones. Furthermore, in a brain showing many complex convolutions, sulci are less deeply hollowed because of the compression of gyri and therefore the brain leaves fewer imprints of the sulci on the cranial bones. No significant difference appears to separate the thickness of the meninges in both extant and extinct Equoidea and so it becomes pertinent to compare digital cranial endocasts from extinct species with the ones from extant Przewalski's in further studies.

Description of the Variation

Cranial Endocast

The cerebral morphology of the domestic horse is already widely known (e.g., Barone 2004). It is now possible to show that the Przewalski's horse presents similar structures (Fig. 1).

Here, the focus is on the description and analysis of the variable structures in the organs of the endocranial cavity. Most of the general measurements of the endocast reveal little variation (Table 2, Online Resource 4); however, the whole volume is quite variable ($570 \pm 33 \text{ cm}^3$). The ratio between cerebellum and cerebrum shows minor variations in all specimens. The cerebrum is roughly eight times the volume of the cerebellum (Table 2).

The different body weight estimations suggest consistent results. The six dental variables from Janis (1990) indicate a mean weight in the studied population of Przewalski's horses of $337 \pm 34 \text{ kg}$. The two variables related to the upper teeth provide a mean weight of $331 \pm 52 \text{ kg}$ (Table 3). Remy's (1998, 2004) equations indicate a weight ranging from $350 \pm 52 \text{ kg}$ (P_1) to $416 \pm 60 \text{ kg}$ (P_2). From these body weights, several estimations of the encephalization quotients were obtained: from 0.84 to 1.29 for dental measurements; from 0.84 to 1.07 for the first equation of Remy (P_1 1998, 2004); and from 0.73 to 0.94 for the second equation of Remy (P_2 1998, 2004).

The surface of the foramen magnum was then measured, as it is needed for the Radinsky EQA (1976). This surface presents a wide variation, unrelated to the sex or the age of the specimens (from 7 to 9 cm^2), which leads to a large EQA range (from 0.95 to 1.51, Table 3). In all of these encephalization quotients, there was a notable variation but two of them suggest an eventual link with ontogeny. Indeed, quotients based on the six dental measurements by Janis (1990) are mostly less than 1 in the seven young individuals (0.84 to 0.97 and only one exceeded 1 with 1.04) whereas the three adults range from 1.11 to 1.15. Quotients calculated from the two dental measurements by Janis (1990) are always less than 1 in the seven young individuals (0.84 to 0.95) whereas the four adults range from 1.06 to 1.29 (Online Resource 5).

The contour of the medulla oblongata, in spite of little variation on its dorso-ventral diameter (Table 2), shows great variation in its shape, ranging from rounded to oval and sometimes slightly pinched (Table 4). The position of the hypophysis is generally stable, except in one specimen (AR, Table 2, Online Resource 4). Here again, the shape presents a large variation, ranging from invisible to highly prominent (Fig. 3, Table 4). In most reconstructed endocasts, the V_1 and V_2 branches of the trigeminal nerve (V) are separated. It means that a bony septum usually separates the two branches, except in some cases (EH and EM, Table 4, Fig. 3). They join the canal that also carries the maxillary artery at different locations (Table 2). The arrangement of the optic nerves (divergence, length of the intracranial track, distance from the trigeminal emergence) is quite variable (Table 2). From a frontal view, these three ducts for nerves and artery (II , V_1 , V_2 , and maxillary artery) can be dorso-ventrally or laterally arranged (Table 4, Fig. 3). The path of the communicating rostral artery leaves an imprint between the olfactory bulbs, which is more or less deep and elongated (Table 2). From a lateral view, the

Table 2 Mean measurements of the brain of *Equus caballus przewalskii*. General measurements, *h*, height; *L*, length; *w*, width; *N/C index*, ratio of height of the neopallium and cerebrum; *R*, right; *LE*, left; *m. obl. DV diam*, diameter of the dorso-ventral cross section of the medulla oblongata

Measurements		Mean	SD	RSD	
General measurements (mm)	encephalon L	153.88	4.40	2.86	
	cerebrum L	131.45	4.79	3.65	
	encephalon h	76.29	3.85	5.04	
	encephalon w	102.27	4.11	4.01	
	cerebellum L	21.66	2.67	12.35	
	neopallium h R	62.97	2.99	4.75	
	neopallium h LE	63.29	2.91	4.60	
	cerebrum h D	76.22	3.00	3.93	
	cerebrum h LE	76.1	2.75	3.62	
	N/C index R	82.6	1.53	1.86	
	N/C index LE	83.16	2.00	2.41	
	m. obl DV diam	29.79	1.71	5.73	
	Ventral measurements	TG-RCA (mm)	26.34	2.95	11.18
		TG-H (mm)	4.61	2.50	54.15
TG-A D (mm)		7.70	2.00	25.91	
TG-A G (mm)		7.86	2.20	28.01	
TG-CH (mm)		14.77	2.45	16.57	
TG-O (mm)		26.34	2.95	11.18	
α optic n. (°)		98.00	12.80	13.10	
optic n. exit (mm)		33.60	2.52	7.51	
TG exit (mm)		32.85	3.05	9.30	
TG emergence (mm)		20.62	2.22	10.77	
Angles and olfactory bulbs	α n./ m. obl. R (°)	158.59	4.30	2.71	
	α n./ m. obl. LE (°)	158.63	4.04	2.55	
	α cbl./ m. obl. (°)	134.27	11.25	8.38	
	Ob free (mm)	9.11	1.62	17.76	
	Ob length (mm)	38.80	1.08	2.79	
	Ob free ratio (%)	23.50	4.20	17.89	
Volumes	α frontal l./ Ob (°)	51.35	9.54	18.58	
	Ob (cm3)	8.9	1.3	14.3	
	cerebrum (cm3)	494.1	31.0	6.3	
	cerebellum (cm3)	66.4	5.2	7.8	
	total (cm3)	625.8	34.7	5.5	
	Ob+Cbr+Cbl (cm3)	569.5	33.2	5.8	
	T-(Ob+Cbr+Cbl) (cm3)	56.2	3.2	5.7	
	Cbl/Cbr (cm3)	0.1	0.0	8.1	

Ventral measurements, see Online Resource 1. Angles and olfactory bulbs, α cbl./ m. obl., angle between cerebellum and medulla oblongata; α frontal l./ Ob, angle between frontal lobes and olfactory bulbs; α n./ m. obl., angle between orbitary nerves and medulla oblongata; further explanations given in Online Resource 1. Volumes, Ob, olfactory bulbs; T-(Ob+Cbr+Cbl), Total volume minus the combined volume of olfactory bulbs, cerebrum and cerebellum; Cbl/Cbr, volumic ratio of the main parts of the brain (cerebellum/cerebrum). SD, Standard Deviation; RSD, Relative Standard Deviation; ? unavailable data. See details of all specimens in Online Resource 2

flexion of the endocast, calculated from the angle between the medulla oblongata and the fifth nerve, is fairly stable (Table 2).

Gyri and sulci from the cerebellum are not distinguishable on digitally reconstructed endocasts (Fig. 1). Parts of the outlines of the paramedian lobe and the paraflocculus are barely distinguishable and appear somewhat variable. From a lateral

view, the medius vermis cerebelli lobe is generally flat but can be more rounded (Table 4, Fig. 3). The angle between the cerebellum and the medulla oblongata can vary (Table 2). This seems linked to the morphology of the medius vermis cerebelli lobe as seen from a lateral view. Specimens where it is rounded present low values whereas, despite one exception (BE, Table 2, Online Resource 4), specimens where it is

Table 3 Mean body weight estimations and encephalization quotients of *Equus caballus przewalskii*. *Lmin*., minimum length; *Lmax*, maximum length; *wmax*, maximum width

Measurements		Mean	SD	RSD
Body weight estimation from dental measurements	m1 Lmin (mm)	2.81	0.13	4.64
	m1 Lmin weight (kg)	495.50	71.68	14.47
	m1 wmax (mm)	1.45	0.15	10.65
	m1 wmax weight (kg)	256.48	81.11	31.62
	m2 Lmin (mm)	2.83	0.14	5.07
	m2 Lmin weight (kg)	381.21	60.39	15.84
	m2 wmax (mm)	1.39	0.11	8.04
	m2 wmax weight (kg)	196.90	50.74	25.77
	M2 Lmax (mm)	2.92	0.24	8.35
	M2 Lmax weight (kg)	370.91	86.49	23.32
	M2 wmax (mm)	2.47	0.07	3.00
	M2 wmax weight (kg)	290.21	42.36	14.60
	Mean weight 6 (kg)	336.67	34.06	10.12
	Mean weight 2 (kg)	330.56	51.53	15.59
Body weight estimation from skull length	skull length (cm)	47.1	2.17	4.61
	body length (cm)	213.4	9.8	4.59
	R1 weight (kg)	349.98	51.99	14.86
	R2 weight (kg)	415.66	59.52	14.32
B.w.e. from f. magnum surf	f. magnum surf. (cm ³)	7.79	0.54	6.95
	EQA	1.23	0.17	13.99
encephale measured volume (cm ³)		570.84	34.74	6.09
EQ weight 6	enceph. vol. e. (cm ³)	580.14	39.37	6.79
	EQ	0.99	0.11	11.20
EQ weight 2	enceph. vol. e. (cm ³)	572.25	60.35	10.55
	EQ	1.02	0.15	14.69
EQ weight R1	enceph. vol. e. (cm ³)	594.61	59.21	9.96
	EQ	0.96	0.08	8.03
EQ weight R2	enceph. vol. e. (cm ³)	666.95	64.00	9.60
	EQ	0.86	0.07	7.73

Mean weight 6, mean weight calculated from the six retained variables; Mean weight 2, mean weight calculated from the two variables relevant for fossil material (M2 Lmax and M2 wmax); Equations linking dental measurements and body weight are from Janis 1990: m1 Lmin: $P = \exp(3.187 \cdot \log_{10}(m1 Lmin) + 1.264)$; m1 wmax: $P = \exp(2.856 \cdot \log_{10}(m1 wmax) + 1.940)$; m2 Lmin: $P = \exp(3.010 \cdot \log_{10}(m2 Lmin) + 1.216)$; m2 wmax: $P = \exp(2.910 \cdot \log_{10}(m2 wmax) + 1.873)$; M2 Lmax: $P = \exp(2.900 \cdot \log_{10}(M2 Lmax) + 1.209)$; M2 wmax: $P = \exp(2.887 \cdot \log_{10}(M2 wmax) + 1.345)$. Ratio between skull length and body length used here is a mean (4.535) of those from literature (4.62, Simpson 1951; 4.35, Bourdelle in Viret 1958; 4.71, Franzen 2010; 4.46, Barone 2004). R1 weight is the weight estimation from the body length according the first equation from Remy 2004: $P1 = 0.0084 \cdot L3.27$, R2 weight is the weight estimation from the body length according the second equation from Remy 2004: $P = 0.019 \cdot L3.15$; B.w.e. from f. magnum surf., Body weight estimation from the foramen magnum surface. EQA, encephalization quotient from Radinsky (Radinsky 1967, 1976; EQ, encephalization quotient from Jerison 1973, calculated from the four precedently estimated weight on dental measurements and skull length; SD, Standard Deviation; RSD, Relative Standard Deviation; ?, unavailable data; /, inapplicable data. See details of all specimens in Online Resource 3

flat present high values. The volume of the cerebellum exhibits only little variation (Table 2).

Among the Przewalski sample group, cerebrum structures are more or less distinguishable, which could indicate a slightly intraspecific variation in the thickness of the meninges. Sulci and gyri are therefore hardly recognizable. However, depending on the specimen, it is possible to identify parts of about twelve sulci on the neopallium, the rhinal fissure, one

sulcus on the rhinencephalon and the fissura longitudinalis cerebri (Fig. 1). On a single specimen, some sulci appear deep and well defined. Therefore, bone probably penetrated further into these sulci than into others, as seen in the frontal area where this lobe is always the best defined. However, it is essential to note that sulci imprints vary in a population and even in a single individual. These sulci can also vary in shape, localization, length or impression (Table 4). They can be well

Table 4 Variation of brain characters in *Equus caballus przewalskii* sample. /, inapplicable data

Characters	AR	BB	BE	CE	EH	EL	EM	MA	PN	SC	SI	SN
Brain base												
Cross-section of the medulla (oval -1-, rounded -2-, pinched -3-)	/	1	3	1	2	1	2	1	1	3	1	1
Hypophysis (not visible -1-, intermediate -2-, prominent -3-)	3	1	3	2	2	2	2	1	2	3	1	2
Bony septum between V ₁ and V ₂ before their exit from the brain (present -1-, absent -2-)	1	1	1	1	2	1	2	1	1	1	1	1
Nerves arrangement (dorso-ventrally -1-, laterally -2-)	2	2	2	2	2	2	2	2	1	2	2	2
Cerebellum												
Medius vermis cerebelli lobe in lateral view (flat -1-, rounded -2-)	1	1	1	2	1	1	1	1	2	1	2	2
Cerebrum												
Blood vessels (some distinguishable -1-, not distinguishable -2-)	2	2	2	2	2	2	2	2	1	2	1	2
Sulcus orbitalis (present -1-, absent -2-)	2	1	1	2	2	2	2	2	2	2	2	2
Sulcus praesylyvia length (stops at the junction of the frontal lobes and olfactory bulbs -1-, continues downwards -2-)	1	2	2	1	1	2	2	1	2	2	2	2
Sulcus praesylyvia orientation (parallel to the olfactory bulbs -1-, backwards -2-)	1	1	1	1	1	1	1	1	1	2	2	1
Sulcus ectosylvia orientation (dorso-ventral -1-, oblique -2-)	1	2	2	2	2	2	2	1	1	2	1	2
Sulcus pseudosylvia imprint (well-imprinted -1-, not distinguishable -2-)	2	1	1	1	1	1	1	1	1	1	2	1
Sulcus pseudosylvia length (reaches half of the brain -1-, stops before it -2-)	/	1	2	1	2	2	1	1	1	1	/	1
Sulcus suprasylvia shape (nearly a straight line -1-, simple curves -2-, sinuous lines -3-)	1	2	3	2	1	3	1	1	3	3	2	2
Sulci ectolateralis and lateralis (both present -1-, both absent -2-)	2	1	2	1	2	2	2	2	2	1	1	1
Sulcus endolateralis (present -1-, absent -2-)	2	1	1	1	1	1	2	1	1	1	2	1
Sulcus endolateralis length (short -1-, extends forward -2-)	1	1	1	1	1	1	1	1	2	1	1	2
Sulcus diagonalis (present -1-, absent -2-)	2	1	2	2	2	2	2	2	2	2	2	2
Posterior rhinal fissure (straight -1-, rounded -2-, sinuous -3-)	3	1	1	3	1	2	1	3	2	1	3	2
Anterior rhinal fissure (present -1-, absent -1-)	1	1	2	1	2	2	2	2	2	2	2	1
Sulcus sagittalis (parallel to anterior rhinal fissure -1-, divergent forward -2-)	1	2	2	2	1	1	1	1	2	1	1	2

Using words “Present” and “Absent” about a sulcus does not portend the existence of these sulci on the brain of the considered specimen but only attested that such sulcus is or is not imprinted on the skull roof of the considered specimen and so do on the digital brain

imprinted on the whole or only represented by a few short parts, such as the sulci ectolateralis and lateralis, which are sometimes confused. Even though the junction between the two parts of the rhinal fissure was never found, it was possible to estimate the proportion of the neopallium and rhinencephalon from the N/C ratio, which was calculated from the posterior part of the rhinal fissure. This proportion does not show great variation and the neopallium occupies about the 4/5th of the height of the cerebrum in all specimens (Table 2). Some blood vessels are distinguishable by the nuchal part of the digital cerebrum and might correspond to the nuchal branch of the middle cerebral artery (Table 4). There is little variation in the volume of the cerebrum (Table 2).

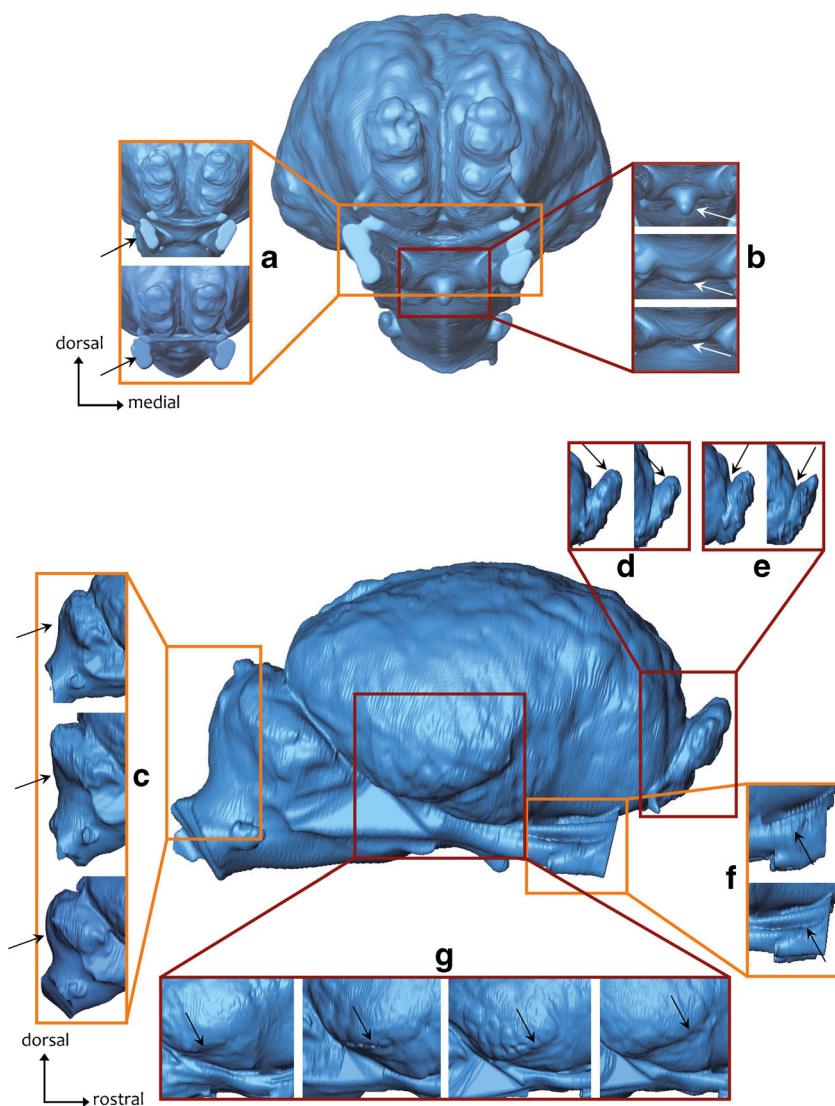
In the extant brain, olfactory bulbs are separated from the brain, although not by bony walls, and they are only linked to the brain at the level of the olfactory peduncles (Fig. 1). On the reconstructions, the bulbs seem closely attached to the digital brain endocast. Their whole length as measured from a dorsal aspect shows little variation (Table 2, Fig. 3). Their dorsal surface makes an angle with the frontal lobes that is more variable, as is their volume (Table 2, Fig. 3). Numerous tubercles were noted, corresponding to the bundles of olfactory fibers (cranial nerve I), which cross the cribriform plate of the ethmoid bone. Moreover, olfactory bulbs show four large

protuberances more or less rounded, long and thick on their rostral side.

Petrosal

Despite some differences, the petrosal morphology of *E. c. przewalskii* is rather similar to that of *E. c. caballus* (e.g., O’Leary 2010) (Fig. 4). The reconstruction of the mastoid is the most affected by the low resolution because of its similar bone density with the closely linked squamosal bone. Thus, the maximal width of the petrosal bone has been measured without the mastoid. This measurement shows little variation (Table 5). The anterior edge of the petrosal is very variable and can have a variable epitympanic wing (Table 6, Fig. 5). The distance between the slit foramen of the vestibular aqueduct and the oblong foramen of the cochlear aqueduct presents little variation (Table 5). The large and flat tegmen tympani extends in an anterior process on specimens with sufficient resolution but stops abruptly on others probably due to a reconstruction artefact. The tegmen tympani show a more or less deeply marked groove of the inferior petrosal sinus, which joins the internal jugular vein in the occipito-spheno-temporal hiatus at the jugular foramen level (Table 6, Fig 5). The internal acoustic meatus presents various sizes and morphologies

Fig. 3 Variation of some characters of the digital brain endocast of *Equus caballus przewalskii*. **a, b** Digital brain endocast in coronal view. **c–g** Digital brain endocast in right lateral view. **a** Nerves arrangement. **b** Hypophysis shape. **c** Medius vermis cerebelli shape. **d** Length of the free part of the olfactory bulbs and **e** their angle with frontal lobes. **f** Bony septum between V_1 and V_2 . **g** Posterior rhinal fissure shape



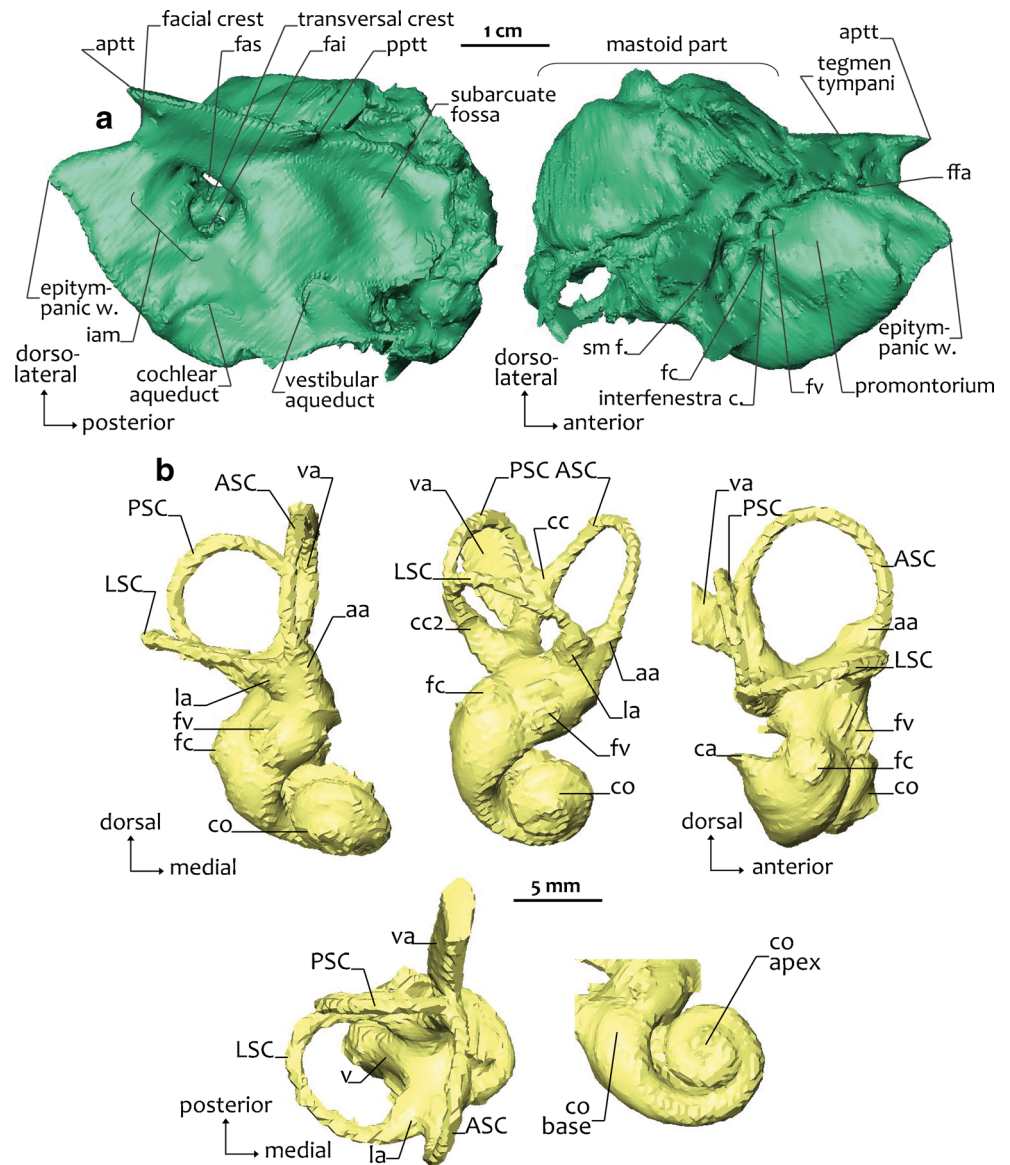
(Tables 5 and 6, Fig. 5, Online Resource 6). In spite of the lack of resolution, the bony bridges that separate the nerves and form the four parts of the meatus show some variations in their forms and positions. The size, morphology, and elongation and depth of the subarcuate fossa are highly variable (Table 6, Fig. 5). The shape of the outline of the promontorium also varies, from ovoid to a sharper form due to a straight posterior edge.

Bony Labyrinth

As for the petrosal, the bony labyrinth morphology of *E. c. caballus* has already been described (e.g., Ekdale 2013). It looks similar to that of *E. c. przewalskii* in spite of some differences (Fig. 4). On average, the anterior canal (ASC) presents the greatest height (Online Resource 7, Table 7). It is higher than it is wide, whereas the lateral canal (LSC) is slightly wider than it is high (Table 7). The latter, and above all, the posterior canal (PSC) are somewhat rounded (see the

h/w ratio in Table 7). However, these measurements are very variable when it comes to details; some individuals can have canals of similar height or width, or an ASC that is wider than it is high, or a PSC that is not so rounded, etc. (Table 7). The transversal diameter or the radius of the semicircular canals could not be measured on these bony labyrinths, because they are eroded due to the low resolution. The PSC is often the longest canal, although the three semicircular canals could also be of similar length (Table 7, Online Resource 7). However, this assessment is not always true because six specimens do not show this (Online Resource 7). On average, the ASC and LSC show similar lengths but they can differ by 2 mm (Table 7, Online Resource 7). Semicircular canals are not strictly orthogonal, but frequently set at slightly acute angles (Table 7, Online Resource 7). The angle between the ASC and the LSC in particular exhibits a great range, with values from 70 to 90° depending on specimens (Table 7, Online Resource 7). The common crus height shows little variation but some extreme values (Table 7; from 3.8 to 6.1 mm, Online Resource

Fig. 4 Digital reconstructions of right petrosal bone (specimen BE) and right bony labyrinth (specimen EM) of *Equus caballus przewalskii*. **a** Cerebellar view (left) and tympanic view (right) of a petrosal. *aptt*, anterior process of tegmen tympani; *epitympanic w.*, epitympanic wing; *fai*, foramen acousticum inferius; *fas*, foramen acousticum superius; *fc*, fenestra cochleae; *ffa*, foramen of fallopian aqueduct; *fv*, fenestra vestibuli; *iam*, internal acoustic meatus; interfenestra *c.*, interfenestra crest; *pptt*, posterior process of tegmen tympani; *sm f.*, stylomastoid foramen. **b** On the top, from left to right, Anterior view, Anterior three-quarters view, Lateral view. On the bottom, from left to right, Posterior view, Cochlea viewed down axis of rotation. *aa*, anterior ampulla; *ASC*, anterior semi-circular canal; *ca*, cochlear aqueduct; *cc*, common crus; *cc2*, second common crus; *co*, cochlear; *fc*, fenestra cochleae; *fv*, fenestra vestibuli; *la*, lateral ampulla; *LSC*, lateral semi-circular canal; *PSC*, posterior semi-circular canal; *v*, vestibule; *va*, vestibular aqueduct



7). The PSC and the LSC seem to form a second, common crus, but this could be a reconstruction artefact due to the weak resolution and the subsequent loss of some details (Fig. 4). On the best virtual slides of the sample a beginning of separation

Table 5 Measurements of the petrosal bone of *Equus caballus przewalskii*. m h, internal acoustic meatus height; m w, internal acoustic meatus width; l, left; max. width, maximal width; r, right; fva-fca, distance between vestibular aqueduct and cochlear aqueduct foramens

Measurements	Mean r	Mean l	Mean	SD	RSD
m h (mm)	7.33	7.12	7.22	0.91	12.57
m w (mm)	7.40	7.38	7.39	0.56	7.58
fva-fca (mm)	9.90	9.75	9.82	0.94	9.59
max. width (mm)	13.85	13.78	13.81	1.38	9.96

SD, Standard Deviation; RSD, Relative Standard Deviation. See details of all specimens in Online Resource 4

was observed but nothing on the worst ones (e.g., BB, CE, and SC). The resolution made it impossible to focus on the sharing of a part of a bony canal by the PSC and LSC. It also could be just an artefact due to the closeness of both the LSC and PSC. The bony channel for the aqueduct of the vestibule is a wide conduit from its junction with the vestibule (Fig. 4). It forms a slightly variable angle with the common crus (Table 7). A distance showing only a small amount of variation (Table 7) separates the vestibular and cochlear fenestrae. The vestibule presents a tiny constriction allowing the distinction of the elliptical recess from the spherical recess of the vestibule. The bending of the bony labyrinth was estimated with the help of two angles: the angle between the common crus and the first turn of the cochlea and angle between the LSC and the cochlear canal. Both show small variations (Table 7). The cochlear canal has 1.75 turns (Table 7) and its length is quite stable. From the apex, the turns are first joined together and

Table 6 Variation of petrosal characters in *Equus caballus przewalskii* sample

Characters	BB r	BB l	BE r	BE l	CE r	CE l	EH r	EH l	EL r	EL l	EM r	EM l	MA r	MA l	PN r	PN l	SC r	SC l	SI r	SI l	SN r	SN l
Anterior edge of the petrosal (flat, without epitympanic wing -1-, rounded, without wing -2-, smooth wing -3-, sharp wing -4-)	4	4	4	3	2	3	3	3	3	3	2	2	3	3	4	4	4	3	1	1	3	3
Groove of the inferior petrosal sinus (shallow -1-, intermediate -2-, deep -3-)	1	1	3	3	1	1	3	2	2	3	3	3	2	2	2	2	3	3	3	3	2	2
Internal acoustic meatus shape (quadrangular -1-, moon shaped -2-, triangular -3-)	1	1	2	2	1	3	1	1	1	1	3	1	1	1	1	1	2	2	3	3	1	2
Fossa subarcuata shape (ovoid with a larger posterior part -1-, oval -2-)	1	1	2	2	2	2	2	1	2	1	2	1	1	1	1	1	1	1	2	2	2	2
Fossa subarcuata size (small -1-, large and extends forward -2-)	1	1	1	1	2	2	2	2	1	1	1	1	2	2	1	1	1	1	1	1	1	1
Fossa subarcuata elongation (along ventromedial-dorsolaterally axis -1-, along antero-posterior axis -2-)	1	1	2	2	1	1	1	1	1	1	1	1	1	1	1	1	1	1	1	1	1	1
Fossa subarcuata depth (shallow -1-, deep -2-)	1	1	2	2	1	1	1	1	2	2	2	2	2	2	2	2	1	1	2	2	2	2

R, right; L, left

then they separate (Fig. 4). The location of the separation is also quite stable. To estimate the contribution of the two parts of the bony labyrinth to the volume, namely the cochlea and vestibule plus the semicircular canals, ratios were calculated (absolute values are not considered because the resolutions are not equal depending on the specimen). Therefore, the cochlea contributes to about half of the whole volume of the bony labyrinth (Table 7). Finally, according to the method described by Manoussaki et al. (2008), horses studied here would have their low-frequency limit around 367±52 Hz (from 279 to 456 Hz) (Table 7). As a comparison, Heffner and Heffner (1983) obtained a very different measurement on living horses: 55Hz.

Squamoso-Parietal Conduit

The reconstruction of the squamoso-parietal conduit is irregular because of the low resolution of the virtual slides and its complex morphology (Online Resource 8). A large conduit is separated into three regions: the temporal sinus (1), presenting an intraosseous path on the lateral parts of the endocranial cavity at the level of the junction between cerebellum and cerebrum; the transverse (2) and communicating (3) sinuses, which are closely applied against the cranial endocast without any bony wall between them. The transverse sinus joins the dorsal sagittal sinus and the communicating sinus joins both temporal sinuses. The squamoso-parietal conduit leads to several foramina: the post-glenoid foramen, mastoid foramen, and the numerous squamoso-parietal perforations. All specimens share this configuration.

Three-Dimensional Geometric Morphometry

Cranial Endocast

Forty-seven bilateral landmarks and nine midsagittal landmarks (56 altogether) were placed on the 11 better preserved digital endocasts, including 27 landmarks of type I (homologous points), 21 of type II (geometric points), and eight of type III (constructed points) (Online Resource 9). The axes 1, 2, and 3 of the PCA expressed 49.3 % of the total variation inside the sample (respectively 18.2, 16.5 and 14.6 %). The rest of the variation was gradually distributed along seven other axes. These results show that the structuring of the data depended on three major axes whereas the relative weakness of these axes suggested a multidirectional variation. This distribution of the variation was to be expected in a single species and a fortiori in a single population, where the variation should not be very marked. Therefore, only half of the variation could be interpreted. The other half was highly scattered and thus each axis accounted for a small amount of variation, each of which is insignificant when considered separately. All but three specimens are grouped together (CE, EL, and EM) displaying

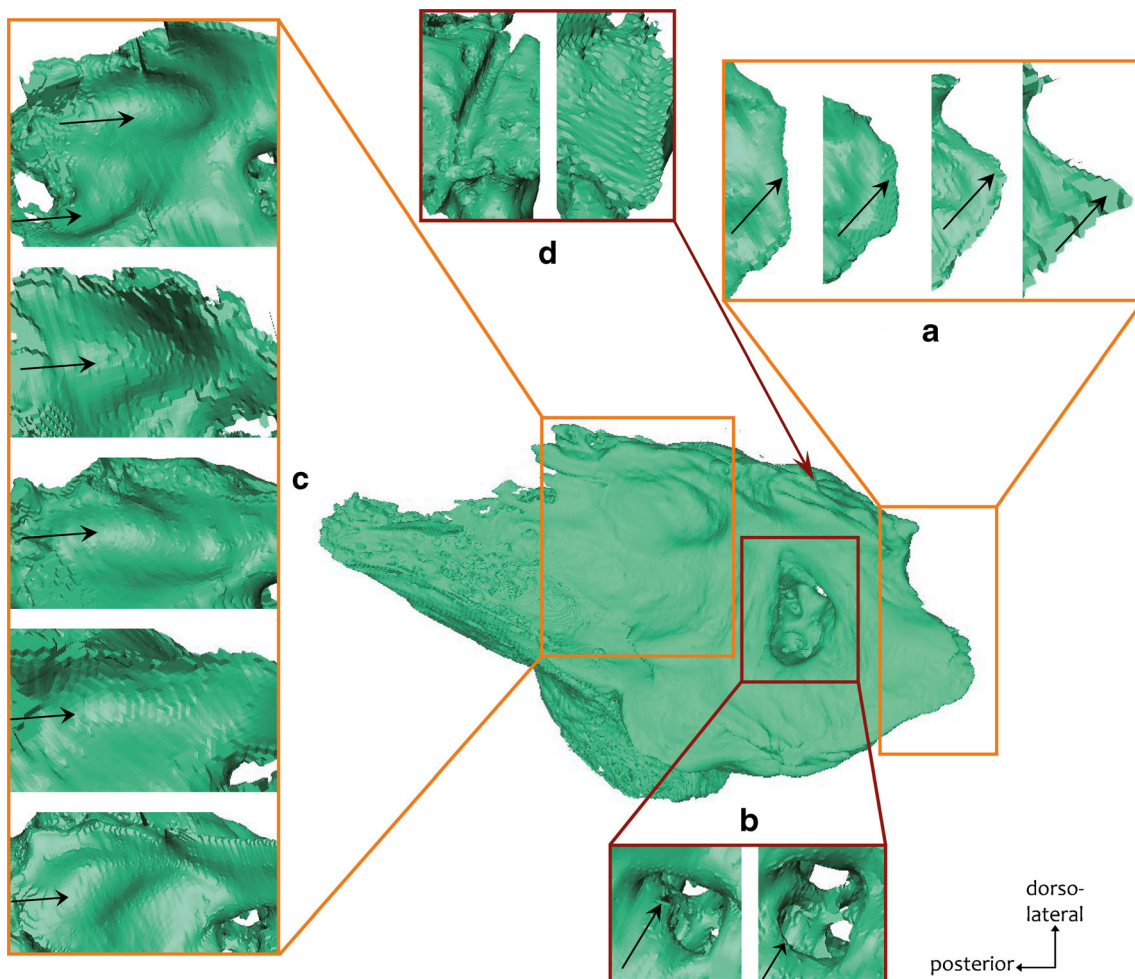


Fig. 5 Variation of some characters of the petrosal bone of *Equus caballus przewalskii*. **a–c** Petrosal in cerebellar view. **d** Petrosal in dorso-lateral view. **a** Epitympanic wing. **b** Internal acoustic meatus shape. **c** Fossa subarcuata shape, size and deepness. **d** Groove of the inferior petrosal sinus

extreme values (Fig. 6, Online Resource 10). In the three-dimensional morphological space defined here, it was impossible to separate individual ages or sexes but a larger range of variation in females was observed (Fig. 6, Online Resource 10). This result is nuanced because of the potentially biased sample of only four males compared to seven females. All of the variation seen in the Przewalski endocast sample is mainly explained by variation in the location of the end of the imprint of the rhinal fissure, an occipital pinch (PC1), the frontal and occipital areas switch (PC2), the compression of the medulla oblongata, and the degree of the extension of the anterior half of the endocast (PC3) (Fig. 6, Online Resource 10). The PC1, accounting for 18.2 % of the whole variation, was explained by (1) the relative size of the middle part of the rhinencephalon and the height of the cranial nerves (V_1 and V_2); (2) the length of the imprint of the posterior rhinal fissure associated with the size of the surface of the lateral olfactory gyrus, the size of the sylvian and temporo-occipital areas (these deformations led to switching between an oblong and a pear-like dorsal outline); (3) the length of the olfactory bulbs; and (4) the pinch of the

occipital area from a lateral view (Fig. 6, Online Resource 10). The PC2 (16.5 % of the variation) captures (1) the relative size of the frontal area, the olfactory bulbs and the medial area around the sulcus endolateralis associated with the size of the occipital and temporal areas; (2) the size of the paraflocculus lobes of the cerebellum; (3) the curved shape of the cranial nerves (V_1 and V_2) associated with the curved shape of the ventral part of the rhinencephalon; and (4) the angle between the olfactory bulbs and the cerebrum (Fig. 6, Online Resource 10). The PC3 (14.6 % of the variation) describes (1) the longitudinal shape of the medulla oblongata (the preserved part, up to the hypoglossal nerve); (2) the size of the anterior part of the rhinencephalon; (3) the width of the rostral part of the neopallium; and (4) the nuchal convexity of the vermis (Fig. 6, Online Resource 10). On the whole, in all three dimensions, the shape of the cerebellum from a lateral view varies from high and narrow to low and thick. From a nuchal view, the distribution of the neocortical mass varies from the ventral part to the dorsal part of the endocast (Fig. 6, Online Resource 10).

Table 7 Means measurements of the bony labyrinth of *Equus caballus przewalskii*

Measurements	Mean r	Mean l	Mean	SD	RSD
PSC height (mm)	6.73	6.56	6.65	0.62	9.39
width (mm)	6.51	6.52	6.52	0.49	7.58
h/w	1.04	1.01	1.02	0.11	10.36
length (mm)	14.05	13.95	14.00	1.43	10.22
ASC height (mm)	7.58	7.79	7.68	0.60	7.82
width (mm)	6.92	6.89	6.91	0.45	6.56
h/w	1.10	1.13	1.11	0.07	6.38
length (mm)	12.52	12.62	12.57	1.18	9.39
LSC height (mm)	5.80	5.83	5.82	0.22	3.80
width (mm)	5.99	6.06	6.03	0.35	5.76
h/w	0.97	0.96	0.97	0.07	7.45
length (mm)	12.54	12.37	12.45	1.04	8.38
α LSC/ASC ($^{\circ}$)	81.82	81.55	81.68	4.31	5.28
α PSC/ASC ($^{\circ}$)	85.82	87.36	86.59	4.02	4.64
α PSC/LSC ($^{\circ}$)	88.55	88.73	88.64	2.63	2.97
cc h (mm)	4.77	4.74	4.75	0.55	11.62
fv-fc (mm)	3.62	3.45	3.53	0.34	9.62
α cc/coch. ($^{\circ}$)	111.18	111.64	111.41	3.46	3.11
α LSC/coch. can. ($^{\circ}$)	84.27	86.09	85.18	4.96	5.83
α cc/va ($^{\circ}$)	153.82	154.00	153.91	5.44	3.54
cochlea l. (mm)	20.21	20.41	20.31	1.69	8.33
cochlea turns ($^{\circ}$)	644.36	628.09	636.23	27.00	4.24
nb of turns	1.75	1.75	/	/	/
turns sep. ($^{\circ}$)	514.38	492.00	503.19	24.93	4.95
r. attached turns	0.79	0.78	0.78	0.02	3.15
vest. vol. (mm ³)	90.04	88.26	89.15	15.11	16.95
coch. vol. (mm ³)	88.34	90.85	89.60	12.39	13.83
ratio cochlea	49.60	50.94	50.27	3.15	6.27
radii ratio	3.46	3.47	3.46	0.25	7.35
LF limit (Hz)	366	367	367	52	14

α cc/coch., angle between common crus and cochlea; α cc/va, angle between common crus and vestibular aqueduct; α LSC/ASC, angle between LSC and ASC; α LSC/coch. can., angle between LSC and cochlear canal; ASC, anterior semicircular canal; cc h, common crus height; cochlea l., cochlea length; coch. vol., cochlear volume; fv-fc, distance between vestibular and cochlear fenestrae; h/w, ratio between height and width; l, left; LF limit, low-frequencies limit; LSC, lateral semicircular canal; nb of turns, number of turns of the cochlea; PSC, posterior semicircular canal; r, right; r. attached turns, ratio of attached turns; radii ratio, ratio developed by Manoussaki et al. 2008; ratio cochlea, proportion of the cochlea on the whole inner ear; turns sep., turns separation; vest. vol., vestibular volume. SD, Standard Deviation; RSD, Relative Standard Deviation?, unavailable data; /, unapplicable data. See details of all specimens in Online Resource 5

Petrosal

Twenty-six landmarks were placed on the petrosal bone, including 16 landmarks of type I and 13 of type II (Online Resource 11). Petrosal bones are paired elements and

therefore there are twice as many petrosals as digital cranial endocasts. Considered together, the sample might increase and would thus be statistically more relevant. Therefore, an initial analysis was made on isolated right and left petrosals and a second on left petrosals after having mirrored them, complementing the sample of the right petrosals with the aim being to determine the validity of the comparison between left and right petrosals. As in the cranial endocasts, the variation is highly scattered and multidirectional in left petrosals, right petrosals, and in both of these combined (the left ones being mirrored). In both the left and right petrosal PCA, the first four axes are considered to be the more significant. They respectively express 69.6 and 66.7 % of the total variation which is representative only for the considered landmarks in this sample. Five other axes are necessary to express the remainder of the variation. The PCA gathering right petrosals and left mirrored petrosals shows, after PC1, a continuous decrease of the variation along 20 other axes. It makes it difficult to select axes for an interpretation, but the first four axes represent 61.51 % of the whole variation. In this analysis, both petrosals of a single individual could be very close or relatively far away from each other. The whole signal is confused in the petrosal bone because of the low resolution. This has led to a limited definition of the landmarks protocol. Therefore, the landmarks network is not accurate enough to properly describe this form and incoherent distortions arise. On this basis, the software calculates an average form for all specimens, used to visualize distortions due to the variations in the sample. When landmarks are not numerous enough, the form is not well described and there can be a significant difference between the object and the actual specimen it should represent (Fig. 7). This is the case for these petrosal bones. Here, distortions have no meaning. Nevertheless, axes and their expression retain their meaning but represent an undefinable part of the whole variation. The few elements available allow the suggestion that no distinction of sex or age was possible from the petrosal bone. However, the neglected mastoid part might be involved in sexual dimorphism as in the human petrosal where a larger expansion allows a larger muscular insertion in males (e.g., Bernard and Moore-Jansen 2009; Saini et al. 2012).

Bony Labyrinth

Thirty-seven landmarks were placed on the bony labyrinth, including nine landmarks of type I, 11 of type II, six of type III, and 11 semi-landmarks (Online Resource 11). As with petrosal bones, the left bony labyrinths were mirrored and put together with the right bony labyrinths. In the analysis of both sides, the first three axes expressed 48.7 % of the total variation (respectively 29.8, 10.5, and 8.4 %). The remaining variation spread out along 18 other axes. Except for some extreme specimens of right bony labyrinths of EH, EM, and

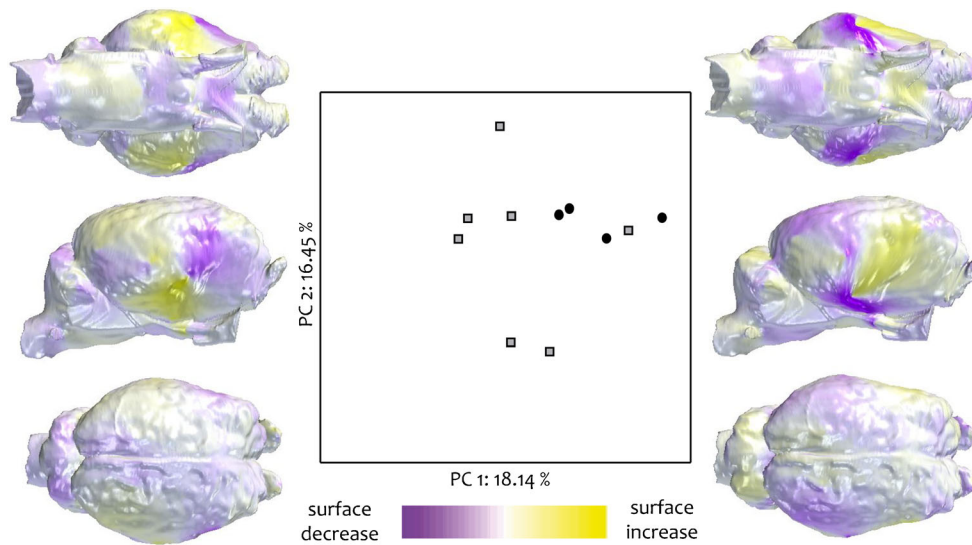


Fig. 6 Principal Components Analysis based on location of 56 landmarks on the brain of *Equus caballus przewalskii*. Specimens distribution along the two major axes. PC, principal component. Grey squares represent females and black circles males. On sides of the graph, see ventral, lateral, and dorsal view of a brain to observe

deformations along the first axis. The more a zone is purple, the more the corresponding surface decreases. The more it is yellow, the more it increases. See Online Resource 10 to observe specimens distribution and deformations along axes 2 and 3

SI, the points are clustered (Fig. 8, Online Resource 12). No distinctions are drawn on the basis of age or sex. Both bony labyrinths of one individual are generally in close proximity. On the whole, the bony labyrinths undergo modifications to their proportions, which affect the size of the cochlear region as opposed to the size of the vestibular and semicircular canals region (Fig. 8, Online Resource 12). On the first axis (PC1), this change impacts (1) the length of the semicircular canals, in particular the ASC and PSC, the length of the common crus, and the vestibular size; (2) the thickness of the cochlear ramp and a slight increase in the number of turns of the cochlear canal (rising from 1.75 to slightly more than 1.75 turns) (Fig. 8, Online Resource 12). PC2 also shows a change in

the proportions but still expresses (1) the width of the turns in the cochlear canal and (2) the length of the common crus (Fig. 8, Online Resource 12). PC3 reflects (1) a tiny variation in the length of the semicircular canals and (2) the length of the cochlear ramp (Fig. 8, Online Resource 12). When only the right bony labyrinths are considered, the first three axes expressed 63.6 % of the whole variation (respectively 36.0, 16.9, and 10.7 %). The rest of the variation spreads out along seven axes. Again, no distinctions could be drawn on the basis of age or sex. Except for EH, EM, and SI, all the specimens are grouped together. On the whole, the same structures are affected as in a general analysis. Specifically, PC1 expresses the same variation although the vestibular size is more stable. PC2

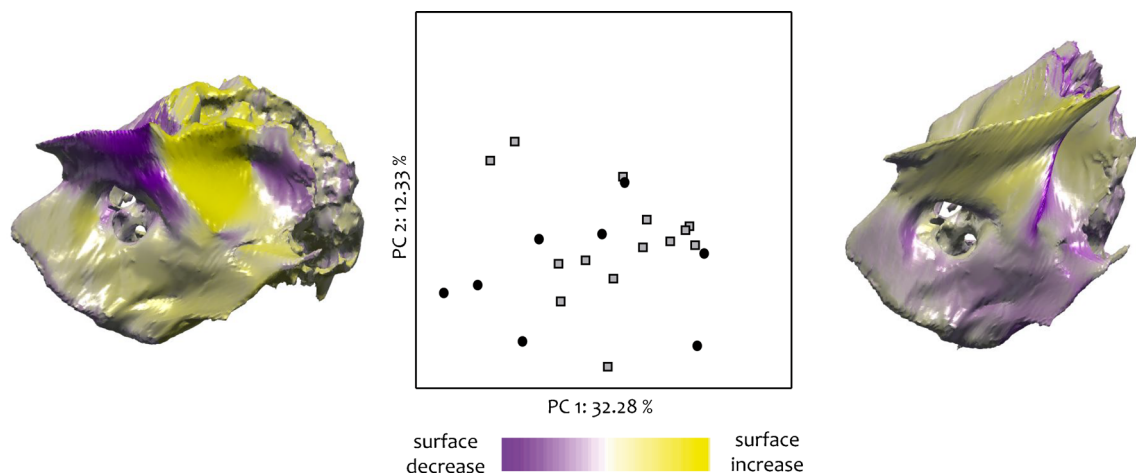


Fig. 7 Principal Components Analysis based on location of 26 landmarks on right and left mirrored petrosal of *Equus caballus przewalskii*. Specimens distribution along the two major axes. PC, principal component. Grey squares represent females and black circles

males. On sides of the graph, see cerebellar view of a petrosal to observe deformations along the first axis. The more a zone is purple, the more the corresponding surface decreases. The more it is yellow, the more it increases

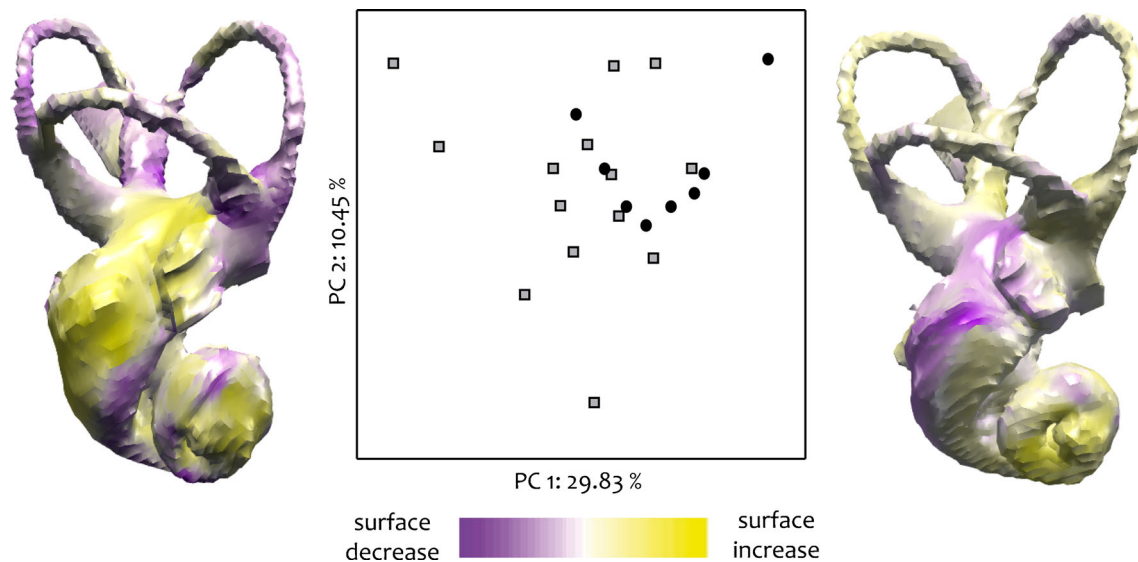


Fig. 8 Principal Components Analysis based on location of 37 landmarks on *right* and *left* mirrored inner ears of *Equus caballus przewalskii*. Specimens distribution along the two major axes. *PC*, principal component. Grey squares represent females and black circles males. On sides of the graph, see anterior three-quarters view of an inner

ear to observe deformations along the first axis. The more a zone is purple, the more the corresponding surface decreases. The more it is yellow, the more it increases. See Online Resource 12 to observe specimens distribution and deformations along axes 2 and 3

and PC3 represent the same variation as in the previous analysis, but the latter also concerned the width of the turns of the cochlear canal. When only left bony labyrinths are considered, the first three axes express 55.9 % of the total variation (respectively 24.5, 17.1, and 14.2 %). The remaining variation spreads out along seven axes. Again, no distinctions are drawn on the basis of age or sex. Specimens are slightly more scattered than in previous analyses and no extremes are found in the individuals studied. However, structures that are affected by both of the main axes, PC1 and PC2, are the same as in both previous analyses. In addition to modifications described in other analyses, PC3 slightly affects the vestibular size. Across the three analyses, the first three principal components express roughly the same variation. This concerns affected structures and the proportion of the total expressed variation. Moreover, no distinction could separate right and left mirrored bony labyrinths in the first analysis to group both sides. Therefore, it is important to compare the right and left (mirrored) bony labyrinths. This is essential from the perspective of studied fossil material, where only a few specimens are available and both sides are not necessarily represented in all individuals.

Discussion

The biometrical, morphological and morphometrical variation data of endocranial structures in a homogenous population of *E. c. przewalskii* have been described here. This work allows the discrimination of 40 variable characters (Table 8).

Origin of the Intraspecific Variation

The structures of cranial endocasts, petrosal bones, and bony labyrinths all vary to a certain degree. In all analyses in this study, the origin of the variation was investigated. This was made possible by the various, accurate data from the skulls of extant individuals obtained for this study (Table 1). To examine sexual variation, four males were compared with seven females. The latter group showed a larger range of variation than the males, but this may be a bias due to the few males accessible. The morphological variation in males falls within the range of the females and it was not possible to distinguish between the two sexes. Several authors have reported cases of sexual differentiation of the brain in birds (Francis 1995; Jacobs 1996; Gahr et al. 1998), in rodents (pocket gophers, Towe and Mann 1995; terrestrial squirrels, Iwaniuk 2001), and, on a smaller scale, in primates (Plavcan and van Schaik 1998). However, unlike *E. c. przewalskii*, all of these mammals show sexual dimorphism in other organs. Horses have only a slight sexual dimorphism in the canine and it is probable that no dimorphism on the endocranial structures should be expected in an almost non-dimorphic species.

As with the other aspects of intraspecific variation, ontogenetic variation has not yet been widely studied. However, one study focused on porpoises is noteworthy (Racicot and Colbert 2013). The authors show, on only a few specimens (five adults but only one juvenile), that important differences can make the distinction between adult and immature endocasts, such as the relative brain size or lobe proportions. Here, to estimate the ontogenetic variation, numerous young individuals from different stages up to sexual maturity were

Table 8 Summary of the main variable endocranial characters, with their range of variation in the *Equus caballus przewalskii* population

Characters	Range of variation	
	Body weight estimations	330.6–415.6 kg
	Encephalization quotient (EQ)	0.84–1.29
Encephalon	Cross-section of the medulla	oval (7); rounded (2); pinched (2)
Brain base	Hypophysis position	backwards TG emergence (11); forward (1)
	Hypophysis shape	not visible (3); intermediate (6); prominent (3)
	Bony septum between V ₁ and V ₂ before their exit from the brain	present (10); absent (2)
	Nerves arrangement	dorso-ventrally (1); laterally (11)
	Angle between both optic nerves	98±13°
Cerebellum	Medius vermis cerebelli lobe in lateral view	flat (8); rounded (4)
	Angle between cerebellum and medulla oblongata	134±11°
Cerebrum	Blood vessels	some distinguishable (2); not any distinguishable (10)
	Neocortical sulci imprint	inter and intra-individual variation
	Sulcus orbitalis	present (2); absent (10)
	Sulcus praesylvia length	short (4); long (8)
	Sulcus praesylvia orientation	parallel to olfactory bulbs (10); backwards (2)
	Sulcus ectosylvia orientation	dorso-ventral (4); oblique (8)
	Sulcus pseudosylvia imprint	well-imprinted (10); not distinguishable (2)
	Sulcus pseudosylvia length	short (3); long (7)
	Sulcus suprasylvia shape	nearly a straight line (4); simple curves (4); sinuous lines (4)
	Sulci ectolateralis and lateralis	both present (5); both absent (7)
	Sulcus endolateralis	present (9); absent (3)
	Sulcus endolateralis length	short (10); long (2)
	Sulcus diagonalis	présent (1); absent (11)
	Posterior rhinal fissure	straight (5); rounded (3); sinuous (4)
	Anterior rhinal fissure	present (4); absent (8)
	Sulcus sagittalis	parallel to anterior rhinal fissure (7); divergent forward (5)
Olfactory bulb	Olfactory bulb free length	9.1±1.6 mm free (23.5±4.2 % from the whole length of olfactory bulb)
	Angle between frontal lobes and olfactory bulbs	51±9.5°
	Olfactory bulbs volume	8.9±1.3 cm ³
Petrosal	Anterior edge of the petrosal	flat without epitympanic wing (2); rounded without wing (3); smooth wing (11); sharp wing (6)
	Petrosal groove	shallow (4); intermediate (8); deep (10)
	Meatus shape	quadrangular (13); moon shaped (5); triangular (4)
	Fossa subarcuate shape	ovoid with a larger posterior part (10); oval (12)
	Fossa subarcuate size	small (16); large and extends forward (6)
	Fossa subarcuate elongation	along ventromedial-dorsolaterally axis (20); along antero-posterior axis (2)
	Fossa subarcuate deepness	shallow (8); deep (14)
Bony labyrinth	Semicircular canals relative length	3 different sizes (14); ASC and LSC of similar size (5); LSC and PSC of similar size (1); ASC and PSC of similar size (2)
	Longest semicircular canal	ASC (2) ; LSC (4); PSC (16)
	Angle between ASC and LSC	82±4° but range of variation from 70 to 90°
	Common crus height	4.8±0.6 mm but range of variation from 3.8 to 6.1 mm

For the meaning of short or length depending on the character, or any descriptive word used here and details on measurements, see Tables 2 to 8. Using words “Present” and “Absent” about a sulcus does not portend the existence of these sulci on the brain of the considered specimen but only attested that such sulcus is or is not imprinted on the skull roof of the considered specimen and so do on the digital brain. Between brackets is the number of specimens sharing the state of character

considered along with several adults, up to an advanced age for a wild horse. These individuals of various ages do not

show any difference between their endocranial morphologies, except for the potential impact of ontogeny on the relative

brain size, as seen in porpoises by Racicot and Colbert (2013). This effect remains hypothetical here because although two encephalization quotients calculations seem to indicate such an ontogenetic variation, the two other methods used to evaluate these quotients do not. Other than this, Anthony and de Grzybowski (1930) showed that the brain, or at least the neopallium, the main structure of the brain, was entirely formed at birth in horses. A newborn shows the same neopallial structures as an adult. After birth these only grow in size, proportional to the increase in body size. The present results are in line with the findings of these authors and extend their conclusions to the remaining parts of the brain, the petrosal, and the bony labyrinth. Moreover, no imprints of bony sutures indicative of an immature individual have been distinguished.

To understand variations in laterality, both right and left paired organs were studied and the left and right areas of the cranial endocast were compared. On the whole, paired organs share the same signal: multi-directional variation, no difference between right and left organs. In both structures, the PCA show some individuals with close-paired objects and others with more remotely paired objects. Intraindividual variation is widely included into intra-population variation that indicates that both sides share the same signal at the scale of a population. Whether variations noted in a single individual between its left and right bony labyrinths could be found in its petrosals (Fig. 9) was also called into question. It seems that no links exist between the two series of data. These results will facilitate comparisons in fossil species where sometimes access to one side of these paired organs is possible.

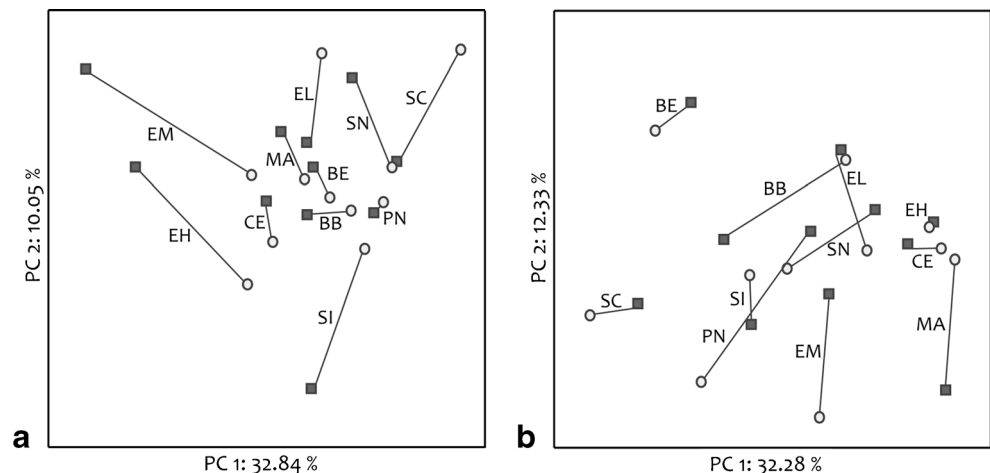
To estimate the effect of genealogy, the genealogical tree of the Przewalski's horses studied here was available (Online Resource 1). It is rather complicated but two groups without close relationships (since their arrival in the Méjean area) are distinguishable. However, their morphology cannot separate them: (1) AR, BB, BE, and PN; (2) CE, EH, EL, EM, MA, SC, SN, and SI.

With the ethological information (Table 1), the impact of endocranial morphology on behavior was called into question, specifically the social position of each individual within the group, although eight out of 12 individuals of the sample used here are young and therefore their social rank in the harem is not yet clearly established. Thus, the information available on social relationships concerns only four individuals and that is too small a sample to properly assess the impact of the cerebral morphology on social rank. Nevertheless, on the four individuals with social data available, no difference was detected that would point to their respective social ranks. Finally, most of the variation noted here does not seem related to sex, age, close relationships between individuals, or social rank within the group but rather seems to be the result of the genetic diversity inside the population. Therefore, this range of variation could now be used for several purposes, such as for ecological or phylogenetic considerations.

Encephalization Quotients

Encephalization quotients are directly dependant on the body weight of the animal and therefore on its estimation. It is well known that these assessments can vary a lot from one method to another. In this study, four different methods were used to estimate the weight of the eleven individuals with preserved crania from the population of *E. c. przewalskii*. They ranged from 331 ± 52 kg to 416 ± 60 kg. The real weight of these individuals was unfortunately unknown, but data about living Przewalski's horses usually range from 200 to 350 kg (Saïdi and Mende 1999). These weight estimations lead to a large range of encephalization quotients, from 0.73 to 1.29. Even if the highest value is deleted (416 ± 60 kg) and only values consistent with the known range of *E. c. przewalskii* weight variation are preserved, the EQ quotient still ranges from 0.84 to 1.29. In most studies about encephalization, only one specimen per species and one method to evaluate body mass are used. This leads to an underestimation of the range of body

Fig. 9 Comparison between left and right structures of *Equus caballus przewalskii* (PCA). **a** Right and left mirrored bony labyrinths. **b** Right and left mirrored petrosals. Dark squares represent right organs and light circles left ones. Lines join right and left structure from a single individual



mass of the considered species, which is not consistent with the reality of a population or with the inaccuracy of the measurements. Such values for encephalization quotients (0.84 to 1.29) are currently considered as very different and are interpreted as a difference in degree of encephalization or evolution, both in old or current papers (e.g., Radinsky 1976; Remy 1978, 2004; Boddy et al. 2012; Benoit et al. 2013b; Kaufman et al. 2013). This study shows that such a variation can be found in a single population and that this kind of interpretation could be inappropriate. Therefore, the practice of using the weight from a single individual to infer the encephalization of a species is questionable. Even if with paleontological data often only one representative of a species is available, it is very important to consider this large variation in order to moderate interpretations. Furthermore, although Jerison's EQ (1973) is the most currently used quotient to estimate the degree of encephalization, and allows authors to make comparisons, it is not universal and some authors use other methods that should prevent comparison (e.g., RMA from Kaufman et al. 2013). However, such comparisons between different methods are current (e.g., Walker 1968; Jerison 1973; Radinsky 1976; Remy 1978, 2004; Janis 1990). The pertinence of such comparisons can be called into question. Nevertheless, encephalization quotients still represent a very interesting parameter; therefore, it is preferable to compare the range of encephalization quotients and not a single value that has no real meaning, as first shown by Radinsky (1974). As with Orliac and Gilissen (2012), several methods should be used to evaluate the weight and several individuals should be used as a basis for estimations so as to take into account the intraspecific weight variation when the material is available. Then, in order to compare different studies, it would be significant to use at least the EQ of Jerison (1973) and other quotients could supplement these data. As for other encephalization quotients, the Radinsky's EQA (1976) was tested here, although his data on Perissodactyla had not been checked. This quotient uses the surface of the foramen magnum to evaluate the body weight. Results obtained in *E. c. przewalskii* showed a great variation, unrelated to sex or age of the specimens and which led to a very large range of EQA. In the absence of results on a large data set of Perissodactyla, it would be better to restrict the use of this encephalization quotient to the five mammal orders tested by Radinsky (1976) and not to use it in Equoidea.

Hearing Abilities Calculation

Manoussaki et al. (2008) developed an original method that could predict the hearing abilities of a mammal based upon some measurements from its cochlear canal. This method was applied to the sample of *E. c. przewalskii* and revealed a low-frequency limit at 367 ± 52 Hz, from 279 to 456 Hz. Heffner and Heffner (1983) realized audiograms on living horses that

indicate a low-frequency limit of 55 Hz, much lower than was found according to the calculation of Manoussaki et al. (2008). As a comparison, it is currently admitted that humans have a low-frequency limit of 20 Hz. The weak sample used in the study of Manoussaki et al. (2008) can be used to explain such an imprecision, highlighted by these authors. Indeed, they tested their method in 13 species, each represented by only one specimen. Furthermore, the lack of any perissodactyls could help to explain this problem. Finally, this method is very difficult to reproduce several times identically and even a tiny difference in measurements can lead to a wide difference in results. Zhang et al. (2007) confirmed the relationship between the curvature of the cochlea and the range of hearing abilities. However, the results obtained by these authors note that the solving of this relationship should be more complex than assumed by Manoussaki et al. (2006, 2008). In these conditions, it seems preferable to avoid this method for Perissodactyla, which were not sampled, and use it carefully in other groups.

Phylogenetic Studies

Phylogenetic studies based on brain characters are still scarce, thus the variation noted here on this organ should be fully exploited before launching such a study. However, few studies begin to check the validity of endocast characters in phylogeny (e.g., Macrini et al. 2007a, b). In the former study, three characters were highlighted that seem variable in this perissodactyl model: the parafloccular shape, which is also based on the fossa subarcuata of the petrosal bone, and two ratios on hypophysis measurements. Macrini et al. (2007b) studied a metatherian mammal displaying a lot of plesiomorphic or different characters compared to an extant eutherian mammal, to the extent that they have few characters in common. This makes inter-comparison of results across studies very difficult. However, both the latter and the present studies may be useful in works about older fossil eutherians, like early Paleogene mammals.

Conversely, descriptions and comparisons have been based on the bony labyrinth and petrosal bone for several decades. Moreover, interest in the structures that are much studied today grew rapidly as a result of the improvement of CT scan technology (e.g., Cifelli 1982; MacPhee 1994; Geisler and Luo 1996; Ladevèze 2006; O'Leary 2010; Orliac 2012; Benoit et al. 2013a; Macrini et al. 2013; Costeur 2014). Nevertheless, some characters described here as variable were used in these studies. Groups of interest vary between studies and perhaps the conclusions drawn in this study cannot be applied to others. However, few studies investigate the intraspecific variation of petrosal bones and bony labyrinths (e.g., Ekdale 2011). In the absence of more studies exploring this variation in detail, it is important to moderate the implications of these characters, in both previous and further studies. As

demonstrated here, characters such as the size or shape of the fossa subarcuata, the presence and shape of the epitympanic wing, or the relative size of semicircular canals are to be cautiously determined because of the great variation found in these structures, at least in a single population of equoids. These characters were scored in phylogenetic studies on other groups of mammals, such as metatherians (Ladevèze 2006), artiodactyls (Geisler and Luo 1996; O’Leary 2010; Orliac 2012), condylarths (Cifelli 1982), or afrotheres (MacPhee 1994; Benoit et al. 2013a). Other comparative work (Costeur 2014) suggested that presence or absence of vascular grooves on the tegmen tympani or the number of turns of the cochlea should bear a clear signal in ruminants. In the present study, in Przewalski’s horse, it is not, but rather bears some variation. All of these works pertain to orders of mammals other than perissodactyls. However, given the new results here, all endocranial characters exhibiting variation in this study must be considered cautiously in further phylogenetic analyses. Moreover, it is important to check this variation in groups other than perissodactyls to get a better comprehension of the variation of endocranial structures. Thus, a recent study (Costeur 2014) compared some ruminants and showed variation on the angle between semicircular canals, as in Przewalski’s horse. Such further works are indispensable in order to extend the knowledge of variation of these structures and increase the resolution of analyses.

Conclusion

So far, few data are available to understand morphological variations of different parts of the still poorly mapped region of the endocranium. In this study, variation in the main parts of the endocranium was investigated. Analyses presented here allow (1) a view of a typical variation in endocranial structures in Equoidea; (2) the classification of morphological variations depending on their range and impact on studied structures; (3) the visualization of whole morphological changes within a single population; and (4) the observation in a three-dimensional morphological space of the distribution of paired organs that belong to a single individual (petrosals and bony labyrinths). The way to use different encephalization quotients is called into question, as is the index establishing hearing abilities. Finally, a list of variable characters has been identified for cranial endocasts, petrosals, and bony labyrinths (Table 8). They should be considered with caution in further phylogenetic studies, at least in Equoidea. It will be necessary to perform such studies in other mammal orders currently studied for their endocranial parts. These considerations could bring new resolution to phylogenetic trees of fossil species in subsequent analyses. Furthermore, some regions seem very affected by morphological variations whereas others show a striking stability. This differential expression of the variation

conceivably reflects different ecological or developmental constraints, which should also be investigated in further studies. Knowing that these constraints can evolve, it follows that variation should also be subject to changes over time. To further refine studies using neurocranial variation data on fossil species, it is important to compare data from the Przewalski’s horse population with some fossil individuals. Such studies would help to develop an eventual evolution of the neurocranial variation in these mammals over the Cenozoic.

Acknowledgments First, we want to thank Claudia Feh and the TAKH association for the gracious loan of all the Przewalski skulls studied in this work and all information about the life of these individuals. CT scans of the Przewalski’s horses have been possible with the assistance of the CHU Lapeyronie (Montpellier), which provided the tomograph and the technicians. To scan the two freshly cut horse heads, we also appealed to a veterinarian, Laure Poujol (veterinary clinic of Celleneuve, Montpellier), for whose help we are grateful. We are very grateful to Renaud Lebrun from the University of Montpellier who trained one of us (LD) in the use of morphometric software. Finally, we thank the two anonymous reviewers who contributed to improving the manuscript. This work has been supported by the ANR funding project Palasiafrica. This is the publication ISEM n° 2015–051.

References

- Achilli A, Olivieri A, Soares P, Lancioni H, Kashani BH, Peregó UA, Nergadze SG, Carossa V, Santagostino M, Capomaccio S, Felicetti M, Al-Achkar W, Penedo CT, Verini-Supplizi A, Houshmand M, Woodward SR, Semino O, Silvestrelli M, Giulotto E, Pereira L, Bandelt H-J, Torroni A (2012) Mitochondrial genomes from modern horses reveal the major haplogroups that underwent domestication. *Proc Natl Acad Sci USA* 109(7):2449–2454
- Anthony R, Grzybowski J de (1930) Le *neopallium* des Equidés. Étude du développement de ses plissements. *J Anat* 64(2):147–169
- Avizo Software (2010) VSG Website [Online] (Updated 2015). Version 7. Available at: <http://www.fei.com/software/avizo3d/>
- Barone R (2004) Anatomie comparée des mammifères domestiques. Tome 6 : Neurologie I. Système nerveux central. Vigot, Paris
- Benoit J, Adnet S, El Mabrouk E, Khayatu H, Ben Haj Ali M, Marivaux L, Merzeraud G, Mériegeaud S, Vianey-Liaud M, Tabuce R (2013a) Cranial remain from Tunisia provides new clues for the origin and evolution of Sirenia (Mammalia, Afrotheria) in Africa. *PLoS ONE* 8(1):1–9
- Benoit J, Crumpton N, Mériegeaud S, Tabuce R (2013b) A memory already like an elephant’s? The advanced brain morphology of the last common ancestor of Afrotheria (Mammalia). *Brain Behav Evol* 81(3):154–169
- Bernard KA, Moore-Jansen PH (2009) Quantifying male and female shape variation in the mastoid region of the temporal bone. Proceedings of the 5th Annual GRASP Symposium, Wichita State University, 80–81
- Boddy AM, McGowen MR, Sherwood CC, Grossman LI, Goodman M, Wildman DE (2012) Comparative analysis of encephalization in mammals reveals relaxed constraints on anthropoid primate and cetacean brain scaling. *J Evol Biol* 25:981–994
- Bookstein FL (1997) Landmark methods for forms without landmarks: morphometrics of group differences in outline shape. *Med. Image. Anal* 1:225–243
- Brochu CA (2000) A digitally-rendered endocast for *Tyrannosaurus rex*. *J Vertebr Paleontol* 20(1):1–6

- Cifelli RL (1982) The petrosal structure of *Hyopsodus* with respect to that of some other ungulates, and its phylogenetic implications. *J Paleontol* 56(3):795–805
- Costeur L (2014) The petrosal bone and inner ear of *Micromeryx flourensianus* (Artiodactyla, Moschidae) and inferred potential for ruminant phylogenetics. *Zitteliana B* 32:1–16
- Cuvier G (1836) Recherches sur les ossements fossiles où l'on rétablit les caractères de plusieurs animaux dont les révolutions du globe ont détruit les espèces. D'Ocagne, Paris
- Danilo L, Remy JA, Vianey-Liaud M, Marandat B, Sudre J, Lihoreau F (2013) A new Eocene locality in southern France sheds light on the basal radiation of Palaeotheriidae (Mammalia, Perissodactyla, Equoidea). *J Vertebr Paleontol* 33(1):195–215
- David R, Droulez J, Allain R, Berthoz A, Janvier P, Bennequin D (2010) Motion from the past. A new method to infer vestibular capacities of extinct species. *C R Palevol* 9(6–7):397–410
- Dechaseaux C (1962) Cerveaux d'animaux disparus. Masson, Paris
- Dietrich WO (1936) Die Huftiere aus dem Obereozän von Mähringen auf der Ulmer Alb. *Palaeontographica* 83A:163–209
- Dong W (2008) Virtual cranial endocast of the oldest giant panda (*Ailuropoda microta*) reveals great similarity to that of its extant relative. *Naturwissenschaften* 95:1079–1083.
- Edinger T (1948) Evolution of the horse brain. *Geol Soc Am Mem* 25:1–177
- Ekdale EG (2010) Ontogenic variation in the bony labyrinth of *Monodelphis domestica* (Mammalia: Marsupalia) following ossification of the inner ear cavities. *Anat Rec* 293:1896–1912
- Ekdale EG (2011) Morphological variation in the ear region of Pleistocene Elephantimorpha (Mammalia, Proboscidea) from central Texas. *J Morphol* 272:452–464
- Ekdale EG (2013) Comparative anatomy of the bony labyrinth (inner ear) of placental mammals. *PLoS ONE* 8(6):1–100
- Francis RC (1995) Evolutionary neurobiology. *Tree* 10(7):276–281
- Franzen JL (1968) Revision der Gattung *Palaeotherium* Cuvier, 1804 (Palaeotheriidae, Perissodactyla, Mammalia). Dissertation, Albert-Ludwigs Universität zu Freiburg i, B:2 vol
- Franzen JL (2010) The Rise of Horses: 55 Million Years of Evolution. Johns Hopkins University Press, Baltimore
- Froehlich DJ (1999) Phylogenetic systematics of basal perissodactyls. *J Vertebr Paleontol* 19(1):140–159
- Gahr M, Sonnenschein E, Wickler W (1998) Sex difference in the size of the neural song control regions in a duetting songbird with similar song repertoire size of males and females. *J Neurosci* 18(3):1124–1131
- Geisler JH, Luo Z (1996) The petrosal and inner ear of *Herpetocetus* sp. (Mammalia, Cetacea) and their implications for the phylogeny and hearing of archaic mysticetes. *J Paleontol* 70(6):1045–1066
- Gorgas M (1966) Betrachtung zur Hirnschädelkapazität zentralasiatischer Wildsäugetiere und ihrer Hausformen. *Zool Anz* 176:227–235
- Gunz P, Mitteroecker P, Bookstein FL (2005). Semilandmarks in three dimensions. In: Slice DE (ed) *Modern Morphometrics in Physical Anthropology*. Kluwer Academic/Plenum Publishers, New York, pp 73–98
- Heffner RS, Heffner HE (1983) Hearing in large mammals: horses (*Equus caballus*) and cattle (*Bos taurus*). *Behav Neurosci* 97(2): 299–309
- Hooker JJ (1989) Character polarities in early perissodactyls and their significance for *Hyracotherium* and infraordinal relationships. In: Prothero DR, Schoch RM (eds) *The Evolution of Perissodactyls*. Oxford University Press, New York, pp 79–101
- Hooker JJ (1994) The beginning of the equoid radiation. *Zool J Linn Soc* 112:29–63
- Horner JR, Goodwin MB (2009) Extreme cranial ontogeny in the upper Cretaceous dinosaur *Pachycephalosaurius*. *PLoS ONE* 4(10):1–11
- Iwaniuk AN (2001) Interspecific variation in sexual dimorphism in brain size in Nearctic ground squirrels (*Spermophilus* spp.). *Can J Zool* 79: 759–765
- Janis CM (1990) Correlation of cranial and dental variables with body size in ungulates and macropodoids. In: Damuth J, Macfadden BJ (eds) *Body Size in Mammalian Paleobiology: Estimations and Biological Implications*. Cambridge University Press, Cambridge, pp 255–299
- Jacobs LF (1996) Sexual selection and the brain. *Trends Ecol Evol* 11: 82–86
- Jerison HJ (1973) *Evolution of the Brain and Intelligence*. Academic Press, New York, London
- Jerison HJ (2007) Fossils, brains, and behaviour. In: Watanabe S, Hofman MA (eds) *Integration of Comparative Neuroanatomy and Cognition*, Kei University Press, Tokyo, pp 13–31
- Kaufman JA, Turner GH, Holroyd PA, Rovero F, Grossman A (2013) Brain volume of the newly-discovered species *Rhynchocyon udzungwensis* (Mammalia, Afrotheria, Macroscelidea): implications for encephalization in sengis. *PLoS ONE* 8(3):1–7
- Kruska D (1973) Cerebralisation, Himevolution und domestikationsbedingte Hirngrößenänderungen innerhalb der Ordnung Perissodactyla Owen, 1848 und ein Vergleich mit der Ordnung Artiodactyla Owen, 1848. *Z Zool Syst Evol Forsch* 11:81–103
- Kruska D (1982) Hirngrößenänderungen bei Tylopoden während der Stammesgeschichte und in der Domestikation. *Verh Zool Ges*: 173–183
- Kruska D (1987) How fast can total brain size change in mammals. *J Hirnforsch* 28(1):59–70
- Kruska D (1988) Effects of domestication on brain structure and behavior in mammals. *Hum Evol* 3(6):473–485
- Kruska D (2005) On the evolutionary significance of encephalization in some eutherian mammals: effects of adaptative radiation, domestication and feralization. *Brain Behav Evol* 65:73–108
- Kruska D (2007) The effects of domestication on brain size. In: Krubitzer L, Kaas J (eds) *Evolution of Nervous Systems*. Vol. 3 Mammals. Academic Press, New York, pp 143–153
- Ladevèze S (2006) Petrosal bones of metatherian mammals from the late Paleocene of Itaboraí (Brazil), and a cladistic analysis of petrosal features in metatherians. *Zool J Linn Soc* 150:85–115
- Lebrun R, de Leon MP, Tafforeau P, Zollikofer C (2010) Deep evolutionary roots of strepsirrhine primate labyrinthine morphology. *J Anat* 216:368–380
- MacPhee RDE (1994) Morphology, adaptations and relationships of *Plesiorcycteropus*, and a diagnosis of a new order of eutherian mammals. *Bull Am Mus Nat Hist* 220:1–214
- Macrini TE (2009) Description of a digital cranial endocast of *Bathygenys reevesi* (Merycoidodontidae; Oreodontidae) and implications for apomorphy-based diagnosis of isolated, natural endocasts. *J Vertebr Paleontol* 29(4):1199–1211
- Macrini TE, Flynn JJ, Ni X, Croft DA, Wyss AR (2013) Comparative study of notoungulate (Placentalia, Mammalia) bony labyrinths and new phylogenetically informative inner ear characters. *J Anat* 223: 442–461
- Macrini TE, Rougier GW, Rowe T (2007a) Description of a cranial endocast from the fossil mammal *Vincelestes neuquenianus* (Theriformes) and its relevance to the evolution of endocranial characters in therians. *Anat Rec* 290:875–892
- Macrini TE, Rowe T, Vandeberg JL (2007b) Cranial endocasts from a growth series of *Monodelphis domestica* (Didelphidae, Marsupalia): a study of individual and ontogenic variation. *J Morphol* 268:844–865
- Manger PR, Pillay P, Maseko BC, Bhagwandin A, Gravett N, Moon D-J, Jillani N, Hemingway J (2009) Acquisition of brains from the African elephant (*Lexodonta africana*): perfusion-fixation and dissection. *J Neurosci Methods* 179:16–21

- Manoussaki D, Chadwick RS, Ketten DR, Arruda J, Dimitriadis EK, O'Malley JT (2008) The influence of cochlear shape on low-frequency hearing. *Proc Natl Acad Sci USA* 105(16):6162–6166
- Manoussaki D, Dimitriadis EK, Chadwick RS (2006) Cochlea's graded curvature effect on low frequency waves. *Phys Rev Lett* 96:1–4
- Mohr E (1959) Das Urwildpferd *Equus przewalskii* Poliakov, 1881. Die Neue Brehm Bücherei, Ziemsen
- Novacek MJ (1982) The brain of *Leptictis dakotensis*, an Oligocene leptictid (Eutheria, Mammalia) from North America. *J Paleontol* 56(5):1177–1186
- Oakenfull EA, Lim HN, Ryder OA (2001) A survey of equid mitochondrial DNA: implications for the evolution, genetic diversity and conservation of *Equus*. *Conserv Genet* 1: 341–355
- Oakenfull EA, Ryder OA (2002) Genetics of equid species and subspecies. In: Moehlman PD (ed) *Equids: Zebras, Asses and Horses: Status Survey and Conservation Action Plan*. World Conservation Union, pp 108–112
- O'Leary MA (2010) An anatomical and phylogenetic study of the osteology of the petrosal of extant and extinct artiodactylans (Mammalia) and relatives. *Bull Am Mus Nat Hist* 335:1–206
- Orlando L, Ginolhac A, Zhang G, Froese D, Albrechtsen A, Stiller M, Schubert M, Cappellini E, Petersen B, Moltke I, Johnson PLF, Fumagalli M, Vilstrup J, Raghavan M, Korneliusen T, Malaspina A-S, Vogt J, Szklarczyk D, Kelstrup C, Vinther J, Dolocan A, Stenderup J, Velazquez AMV, Cahill J, Rasmussen M, Wang X, Min J, Zazula GD, Seguin-Orlando A, Mortensen C, Magnussen K, Thompson JF, Weinstock J, Gregersen K, Roed KH, Eisenmann V, Rubin CJ, Miller DC, Antczak DF, Bertelsen MF, Brunak S, Al-Rasheid KAS, Ryder O, Anderson L, Mundy J, Krogh A, Gilbert MTP, Kjær K, Sicheritz-Ponten T, Jensen LJ, Olsen JV, Hofreiter M, Nielsen R, Shapiro B, Wang J, Willerslev E (2013) Recalibrating *Equus* evolution using the genome sequence of an early middle Pleistocene horse. *Nature* 499:74–78
- Orliac MJ (2012) The petrosal bone of extinct Suoidea (Mammalia, Artiodactyla). *J Syst Paleontol*:1–21
- Orliac MJ, Benoit J, O'Leary MA (2012) The inner ear of *Diacodexis*, the oldest artiodactyl mammal. *J Anat* 221(5):417–426
- Orliac MJ, Gilissen R (2012) Virtual endocranial cast of earliest Eocene *Diacodexis* (Artiodactyla, Mammalia) and morphological diversity of early artiodactyl brains. *Proc R Soc Lond B* 279:3670–3677
- Poliakov IS (1881) *Sistematiceskij obzor polevok, vodjascichsja v cibri. Imperatorskoj Moscow, Akademii Nauk, Zapiski*
- Plavcan JM, Schaik CP van (1998) Intrasexual competition and body weight dimorphism in anthropoid primates. *Am J Phys Anthropol* 103(1):37–68
- Racicot RA, Colbert MW (2013) Morphology and variation in porpoise (Cetacea: Phocoenidae) cranial endocasts. *The Anat Rec* 296:979–992
- Radinsky LB (1967) Relative brain size: a new measure. *Science* 155: 836–838
- Radinsky LB (1974) The fossil evidence of anthropoid brain evolution. *Am J Phys Anthropol* 41(1):15–28
- Radinsky LB (1976) Oldest horse brains: more advanced than previously realized. *Science* 194:626–627
- Remy JA (1967) Les Palaeotheriidae (Perissodactyla) de la faune de mammifères de Fons 1 (Éocene Supérieur). *Palaeovertebrata* 1(1): 1–46
- Remy JA (1972) Étude du crâne de *Pachynolophus lavocati* n. sp. (Perissodactyla, Palaeotheriidae) des Phosphorites du Quercy. *Palaeovertebrata* 5(2):45–78
- Remy JA (1978) Description d'un moulage endocrânien de *Plagiolophus minor* (Palaeotheriidae, Perissodactyla). *Mém Trav EPHE* 5:1–17
- Remy JA (1998) Le genre *Leptolophus* : morphologie et histologie dentaires, anatomie crânienne, implications fonctionnelles. *Palaeovertebrata* 27(1–2):45–108
- Remy JA (2004) Le genre *Plagiolophus* (Palaeotheriidae, Perissodactyla, Mammalia) : Révision systématique, morphologie et histologie dentaires, anatomie crânienne, essai d'interprétation fonctionnelle. *Palaeovertebrata* 33(1–4):17–281
- Röhrs M, Ebinger P (1993) Progressive und regressive Hirngrößenveränderungen bei Equiden. *Z Zool Syst Evol Forsch* 31:233–239
- Röhrs M, Ebinger P (1998) Sind Zooprzewalskipferde Hauspferde? *Berl Munch Tierarztl Wochenschr* 111:273–280
- Rowe T, Brochu CA, Colbert M, Merck JW, Kishi K, Saglam E, Warren S (1999) Introduction to alligator: digital atlas of the skull. *J Vertebr Paleontol* 19(2):1–8
- Rowe T, Macrini TE, Luo Z-X (2011) Fossil evidence on origin of the mammalian brain. *Science* 332:955–957
- Saïdi S, Mende C (1999) L'utilisation des pelouses caussenardes par le cheval de Przewalski. *Mappemonde* 53(1):9–14
- Saini V, Srivastava R, Rai RK, Shamal SN, Singh TB, Tripathi SK (2012) Sex estimation from the mastoid process among North Indians. *J Forensic Sci* 57(2):434–439
- Savage DE, Russell DE, Louis P (1965) European Eocene Equidae (Perissodactyla). *Univ Calif Publ Geol Sci* 56:1–94
- Scannella JB, Horner JR (2010) *Torosaurus* Marsh, 1891, is *Triceratops* Marsh, 1889 (Ceratopsidae: Chasmosaurinae): synonymy through ontogeny. *J Vertebr Paleontol* 30(4):1157–1168
- Shoshani J, Kupsky WJ, Marchant GH (2006) Elephant brain. Part 1: gross morphology, functions, comparative anatomy, and evolution. *Brain Res Bull* 70:124–157
- Silcox MT, Dalmyn CK, Bloch, JI (2009) Virtual endocast of *Ignacius graybullianus* (Paromomyidae, Primates) and brain evolution in early Primates. *Proc Natl Acad Sci USA* 106(27):10987–10992
- Simpson GG (1951) *Horses: the Story of the Horse Family in the Modern World and through Sixty Million Years of History*. Oxford University Press, New York
- Specht M (2007) Spherical surface parametrization and its application to geometric morphometric analysis of the braincase. Dissertation. University of Zürich
- Specht M, Lebrun R, Zollikofer C (2007) Visualizing shape transformation between chimpanzee and human braincases. *Vis Comput* 23: 743–751
- Towe AL, Mann MD (1995) Habitat-related variations in rain and body size of pocket gophers. *J Brain Res* 36(2):195–201
- Viret J (1958) Perissodactyla. In: Piveteau JM (ed) *Traité de Paléontologie*, Vol 6–2, pp. 368–475
- Volf J (2003) Przewalskipferd -ein Wild- oder ein Haustier? *Zool Garten* 73:312–323
- Walker EP (1968) *Mammals of the World*. Johns Hopkins Press, Baltimore
- Weinberg R (1903) Fossile Hirnformen. I. *Anchilophus desmaresti*. *Z Wiss Zool* 74:491–500
- Witmer L, Chatterjee S, Franzosa J, Rowe T (2003) Neuroanatomy of flying reptiles and implications for flight, posture and behaviour. *Nature* 425:950–953
- Zhang Y, Kim CK, Lee K, et al. (2007) Resultant pressure distribution pattern along the basilar membrane in the spiral shaped cochlea. *J Biol Phys* 33(3):195–211